INTERNATIONAL JOURNAL FOR NUMERICAL METHODS IN ENGINEERING
Int. J. Numer. Meth. Engng 2000; **48**:679–720

A continuum Lagrangian sensitivity analysis for metal forming processes with applications to die design problems

Nicholas Zabaras[1,*,†], Yangang Bao[1], Akkaram Srikanth[1] and William Garth Frazier[2]

[1] *Sibley School of Mechanical and Aerospace Engineering, 188 Frank H.T. Rhodes Hall, Cornell University, Ithaca, NY 14853-3801, U.S.A.*
[2] *Air Force Research Laboratory, Materials and Manufacturing Directorate, AFRL/MLMR Building 653, 2977 P Street, Suite 14, Wright-Patterson Air Force Base, OH 45433-7746, U.S.A.*

SUMMARY

A continuum sensitivity analysis is presented for large inelastic deformations and metal forming processes. The formulation is based on the differentiation of the governing field equations of the direct problem and development of weak forms for the corresponding field sensitivity equations. Special attention is given to modelling of the sensitivity boundary conditions that result due to frictional contact between the die and the workpiece. The contact problem in the direct deformation analysis is modelled using an augmented Lagrangian formulation. To avoid issues of non-differentiability of the contact conditions, appropriate regularizing assumptions are introduced for the calculation of the sensitivity of the contact tractions. The proposed analysis is used for the calculation of sensitivity fields with respect to various process parameters including the die surface. The accuracy and effectiveness of the proposed method are demonstrated with a number of representative example problems. In the die design applications, a Bézier representation of the die curve is introduced. The control points of the Bézier curve are used as the design parameters. Comparison of the computed sensitivity results with those obtained using the direct analysis for two nearby dies and a finite difference approximation indicate a very high accuracy of the proposed analysis. The method is applied to the design of extrusion dies that minimize the standard deviation of the material state in the final product or minimize the required extrusion force for a given reduction ratio. An open-forging die is also designed which for a specified stroke and initial workpiece produces a final product of desired shape. Copyright © 2000 John Wiley & Sons, Ltd.

KEY WORDS: sensitivity analysis; die design; metal forming processes; large deformation; plasticity; Lagrangian analysis; optimization

*Correspondence to: Nicholas Zabaras, Sibley School of Mechanical and Aerospace Engineering, 188 Frank H.T. Rhodes Hall, Cornell University, Ithaca, NY 14853-3801, U.S.A.
†E-Mail: zabaras@cornell.edu

Contract/grant sponsor: NSF; contract/grant number: DMII-9522613
Contract/grant sponsor: Materials and Manufacturing Directorate, Air Force Research Laboratory, WPAFB; contract/grant number: TMC96-5835-0018-09-05
Contract/grant sponsor: Alcoa Laboratories

Received 31 March 1999
Revised 20 September 1999

Report Documentation Page

Form Approved
OMB No. 0704-0188

1. REPORT DATE	2. REPORT TYPE	3. DATES COVERED
20 SEP 1999		**00-00-1999 to 00-00-1999**

4. TITLE AND SUBTITLE	5a. CONTRACT NUMBER
A continuum Lagrangian sensitivity analysis for metal forming processes with applications to die design problems	5b. GRANT NUMBER
	5c. PROGRAM ELEMENT NUMBER
6. AUTHOR(S)	5d. PROJECT NUMBER
	5e. TASK NUMBER
	5f. WORK UNIT NUMBER
7. PERFORMING ORGANIZATION NAME(S) AND ADDRESS(ES) **Cornell University,Sibley School of Mechanical and Aerospace Engineering,Materials Process Design and Control Laboratory,Ithaca,NY,14853-3801**	8. PERFORMING ORGANIZATION REPORT NUMBER
9. SPONSORING/MONITORING AGENCY NAME(S) AND ADDRESS(ES)	10. SPONSOR/MONITOR'S ACRONYM(S)
	11. SPONSOR/MONITOR'S REPORT NUMBER(S)

12. DISTRIBUTION/AVAILABILITY STATEMENT
Approved for public release; distribution unlimited

13. SUPPLEMENTARY NOTES

14. ABSTRACT

15. SUBJECT TERMS

16. SECURITY CLASSIFICATION OF:			17. LIMITATION OF ABSTRACT	18. NUMBER OF PAGES	19a. NAME OF RESPONSIBLE PERSON
a. REPORT **unclassified**	b. ABSTRACT **unclassified**	c. THIS PAGE **unclassified**	**Same as Report (SAR)**	**42**	

1. INTRODUCTION

Many metal alloys are currently employed in the manufacture of automotive, aerospace and other hardware components. The high cost of manufacturing critical structural components can be significantly reduced with the development of mathematically and physically sound computational methodologies for process design and control. The complicated nature of polycrystalline materials and the induced changes in their microstructure during processing are among the main challenges that one must consider while developing means for the design and control of bulk forming processes that result in products of desired shape and material state.

The desired objectives for a single forming operation, e.g. in a hot extrusion process, may include one or more of the following criteria: uniform deformation in the final product; minimum required work or extrusion pressure; desired microstructure in the final product; minimum or desired residual stress distribution; minimum deformation and wear of the die; desired shape of the final product; and minimum porosity in the final product. Any of these objectives can theoretically be achieved by appropriate design of the die surface; design of the preform; design of the material state (microstructure) in the initial billet; and appropriate selection of the process parameters (ram speed and pressure history, operating temperature, etc.). However, it is important to note that in a single forming operation there is only a limited control of the material state in the final product that one can achieve using a single stage design and generally a multistage process design is required.

Most deformation process design is currently focussed on trial and error techniques based on previous experience and the results of the direct analysis. A systematic review of such problems is given in Reference [1]. The design approaches reported in this reference are not mathematically rigorous and/or realistic from a material representation point of view. However, a variety of important forming design problems were addressed.

On the other hand, sensitivity analysis and optimization theory, provide a fresh look at these problems and can lead to realistic and accurate designs. Traditional forming design problems that can be analysed as optimization problems are the optimum design of dies, preforms and process parameters. To mathematically address such problems, one needs to calculate the sensitivity of the material state and geometry at various stages of deformation with respect to infinitesimal changes in each of the design variables.

Sensitivity computations can be performed using finite difference approximations and the results of the direct analysis for two nearby design variables. In addition to significant computer resources required for solving the direct problem multiple times, difficulties arise in such calculations from the fact that many direct analysis tools are insensitive to infinitesimal changes in the design variables (e.g. the die surface) and cannot provide accurate sensitivity fields. This is particularly true when the computed sensitivity fields are of the same order of magnitude as the numerical error in the solution of the direct analysis.

In the direct differentiation method, a set of field equations are developed by considering the variation of the continuum or discretized field equations of the direct problem with respect to small changes in design parameters [2–6]. The sensitivity field equations are linear and can be efficiently solved. Direct automatic differentiation can also be applied to evaluate sensitivities [7].

In most of the current developments in the field of sensitivity analysis for large deformation problems, the flow formulation is utilized and emphasis is given to steady-state forming applications [6]. Isothermal as well as non-isothermal deformations have been considered and the sensitivity of various forming processes with respect to shape and material parameters has been studied

[8–10]. Computation of sensitivity coefficients for the purpose of parameter identification for finite elasto-plastic deformations is reported in Reference [11].

Although the last few years have seen an increasing interest in the direct differentiation method for calculating sensitivities, a number of challenges still remain in the accurate and effective computation of sensitivity fields for practical engineering problems that involve frictional contact [12]. A sensitivity analysis for frictional metal forming processes in steady state using a flow formulation is presented in Reference [8] where the effect of variation in the Coulomb friction coefficient on the deformation response is studied. Special contact elements were introduced in the workpiece boundary to handle contact/frictional effects. More recently, sensitivity analysis of a non-steady state open die forging process has been carried out in Reference [13] to study the effect of variation in the height of the initial cylindrical preform in a single stage operation. A shape optimization scheme for non-steady state metal forming processes with applications to preform design in forging is given in References [14, 15]. Applications of optimization techniques to net-shape manufacturing involving forging processes are given in Reference [16]. Other applications to extrusion and forging die design can be found in References [17, 18].

The main objective of this paper is to provide sensitivity field calculations that can be used for accurate forming process design. A Lagrangian sensitivity analysis is developed to include the effects of contact and friction for both steady state and non-steady-state metal forming processes. Emphasis in this paper is given to non-shape forming design problems such as the design of various process parameters. In such problems, for example, one calculates the die surface (for a given reduction or die stroke) that results in desired material properties in the final product or a product of desired shape (e.g. in an open-die forging process).

It is common to discretize the die surface using basis functions (e.g. splines or polynomial functions) assuming that certain constraints are satisfied (e.g. fixed reduction) [19–22]. With such discretizations, a die design problem can be posed as an optimization problem with respect to a finite number of algebraic design parameters. The design parameters are here denoted by the vector $\boldsymbol{\beta}_p = \{\beta_i\},\ i = 1, 2, \ldots, N_p$. Various problem-dependent objective functions are usually written implicitly in terms of the parameters $\boldsymbol{\beta}_p$. Such objective functions may represent for example, the deviation of the resulting material state of the final product from a desired state for the process defined by design parameters $\boldsymbol{\beta}_p$. Similarly, the objective function can be selected to minimize the required work expenditure for the design parameters $\boldsymbol{\beta}_p$.

There are many ways to solve the above class of optimization problems but most commonly a sequential search method is employed starting from a guess solution that is iteratively updated along some specific direction and a given step size [23]. To determine at each optimization iteration the specific search direction and step, one must evaluate the gradient of various fields (material or geometric) involved in the definition of the objective function with respect to design parameters. The interest here is in using a sensitivity analysis for evaluating the gradient of the objective function. With such an analysis, sensitivities of various Lagrangian fields can easily be calculated sequentially in time.

The work reported here is an extension of an earlier work by Zabaras and co-workers [24]. In this work, a continuum sensitivity analysis for hyperelastic viscoplastic deformations was introduced and some die design examples were analysed. The sensitivity fields were defined as directional derivatives of the corresponding Lagrangian fields of the direct analysis. For die design, for example, these directional fields were calculated at a reference die and for a given die perturbation. Appropriate kinematic and constitutive sensitivity problems were defined and the sensitivities of the contact tractions were calculated by assuming Coulomb friction in the contact boundary and

by applying direct differentiation of the impenetrability constraint and contact traction components with respect to the die surface. The sensitivity of the contact pressure was eliminated from these equations with the sensitivity of the normal to the die unit vector expressed in terms of the reference die surface and the die surface variations. Even though the technique introduced in Reference [24] was found to give very good results for simple die design problems, accuracy concerns were raised in many other die and preform design problems [25]. These difficulties were attributed to the explicit manner with which contact was treated in both the direct and sensitivity analyses. Such issues will be addressed in this paper by employing a fully implicit contact scheme and its regularized derivative.

The plan of this paper is the following. At first, a brief introduction of the direct deformation problem is given to set the notation for the sensitivity analysis. A fully implicit augmented Lagrangian algorithm for handling the contact/friction sub-problem of the direct analysis is then presented. The constitutive and kinematic sensitivity problems are briefly reviewed next together with the techniques for their solution. The contact sensitivity algorithm is derived by the direct differentiation of continuum contact and frictional constraints and the implementation of the resulting sensitivity constraints using a penalty formulation. To allow for the differentiability of the continuum contact/frictional constraints, appropriate regularizing assumptions are introduced. The developed contact sensitivity problem is linear and augmentation steps are avoided by appropriate selection of penalty parameters that enforce contact/frictional sensitivity constraints. The paper concludes with an evaluation of the accuracy of the proposed methodology and a presentation of the solution of a number of die design problems in extrusion and open-die forging processes.

2. REVIEW OF A DIRECT LARGE INELASTIC DEFORMATION PROBLEM

2.1. Kinematic and constitutive equations

The basic governing equations for the Lagrangian analysis of the large deformation of isotropic viscoplastic solids are presented here to set the notation for the proposed sensitivity analysis.

Let us denote with $\mathbf{B}_0$ the configuration of the body at time $t=0$ and with $\mathbf{B}_t$ the current body configuration at time t. Consider the location $\mathbf{x}$, in the current configuration $\mathbf{B}_t$, that at time t is occupied by the material point $\mathbf{p}$. Let $\mathbf{X}$ be the location of this particle in the configuration $\mathbf{B}_0$ at time $t=0$. A smooth mapping $\boldsymbol{\phi}$ exists such that

$$\mathbf{x}=\boldsymbol{\phi}(\mathbf{X},t) \tag{1}$$

The deformation gradient $\mathbf{F}$ is then defined by

$$\mathbf{F}=\nabla\boldsymbol{\phi}(\mathbf{X},t) \tag{2}$$

Assuming isothermal conditions, the deformation gradient $\mathbf{F}$ is decomposed as follows:

$$\mathbf{F}=\mathbf{F}^{\mathrm{e}}\bar{\mathbf{F}}^{\mathrm{p}},\quad \det\mathbf{F}^{\mathrm{e}}>0 \tag{3}$$

where $\mathbf{F}^{\mathrm{e}}$ is the elastic deformation gradient and $\bar{\mathbf{F}}^{\mathrm{p}}$ the plastic deformation gradient with $\det\bar{\mathbf{F}}^{\mathrm{p}}=1$. From the polar decomposition of $\mathbf{F}^{\mathrm{e}}$, one can write,

$$\mathbf{F}^{\mathrm{e}}=\mathbf{R}^{\mathrm{e}}\mathbf{U}^{\mathrm{e}} \tag{4}$$

The equilibrium equations can be expressed as,

$$\nabla \cdot \mathbf{P} + \mathbf{f} = \mathbf{0} \quad \forall \mathbf{X} \in \mathbf{B}_0 \tag{5}$$

where $\mathbf{P}(\mathbf{X}, t)$ is the first Piola–Kirchhoff stress and $\mathbf{f}(\mathbf{X}, t)$ is the body force density in the reference configuration $\mathbf{B}_0$. The definition of $\mathbf{P}$ and $\mathbf{f}$ is as follows:

$$\begin{aligned} \mathbf{P}(\mathbf{X}, t) &= \det \mathbf{F}\, \mathbf{T}\, \mathbf{F}^{-\mathrm{T}} \\ \mathbf{f}(\mathbf{X}, t) &= \det \mathbf{F}\, \mathbf{b} \end{aligned} \tag{6}$$

Here, $\mathbf{T}$ is the Cauchy stress and $\mathbf{b}$ the known body force density in the current configuration.

The weak form of the above equilibrium equations is stated as follows: *Calculate* $\boldsymbol{\phi}(\mathbf{X}, t)$ *such that*

$$\int_{\mathbf{B}_0} \mathbf{P} \cdot \frac{\partial \tilde{\mathbf{u}}}{\partial \mathbf{X}}\, \mathrm{d}V_0 = \int_{\partial \mathbf{B}_{n+1}} \hat{\mathbf{t}} \cdot \tilde{\mathbf{u}}\, \mathrm{d}A_{n+1} + \int_{\mathbf{B}_{n+1}} \mathbf{b} \cdot \tilde{\mathbf{u}}\, \mathrm{d}V_{n+1} \tag{7}$$

for every admissible test function $\tilde{\mathbf{u}}$. The hyperelastic constitutive equations are taken as [26],

$$\bar{\mathbf{T}} = \mathscr{L}^{\mathrm{e}}(\bar{\mathbf{E}}^{\mathrm{e}}) \tag{8}$$

where the elastic strain $\bar{\mathbf{E}}^{\mathrm{e}}$ is defined by

$$\bar{\mathbf{E}}^{\mathrm{e}} = \ln(\mathbf{U}^{\mathrm{e}}) \tag{9}$$

and the corresponding conjugate stress $\bar{\mathbf{T}}$ is given as,

$$\bar{\mathbf{T}} = (\det \mathbf{U}^{\mathrm{e}})(\mathbf{R}^{\mathrm{e}})^{\mathrm{T}}\, \mathbf{T}\mathbf{R}^{\mathrm{e}} \tag{10}$$

The isotropic elastic moduli $\mathscr{L}^{\mathrm{e}}$ are defined by

$$\mathscr{L}^{\mathrm{e}} = 2\mathscr{G}\mathscr{I} + (\mathscr{K} - \tfrac{2}{3}\mathscr{G})\mathbf{I} \otimes \mathbf{I} \tag{11}$$

with $\mathscr{K}$ the bulk modulus, $\mathscr{G}$ the shear modulus and $\mathbf{I}$, $\mathscr{I}$, the unit second- and fourth-order tensors, respectively.

A flow rule is given in the form of the evolution of $\bar{\mathbf{F}}^{\mathrm{p}}$ with zero spin of the intermediate configuration [26],

$$\bar{\mathbf{L}}^{\mathrm{p}} = \bar{\mathbf{D}}^{\mathrm{p}} = \dot{\bar{\mathbf{F}}}^{\mathrm{p}}(\bar{\mathbf{F}}^{\mathrm{p}})^{-1} = \sqrt{\frac{3}{2}}\, \dot{\bar{\varepsilon}}^{\mathrm{p}}\, \bar{\mathbf{N}}^{\mathrm{p}}(\bar{\mathbf{T}}', \tilde{\sigma}) \tag{12}$$

where

$$\bar{\mathbf{N}}^{\mathrm{p}}(\bar{\mathbf{T}}', \tilde{\sigma}) = \sqrt{\frac{3}{2}} \frac{\bar{\mathbf{T}}'}{\tilde{\sigma}} \tag{13}$$

the equivalent stress $\tilde{\sigma}$ is given by

$$\tilde{\sigma} = \sqrt{\frac{3}{2}\, \bar{\mathbf{T}}' \cdot \bar{\mathbf{T}}'} \tag{14}$$

with

$$\bar{\mathbf{T}}' = \bar{\mathbf{T}} - \frac{\operatorname{tr} \bar{\mathbf{T}}}{3}\mathbf{I} \tag{15}$$

Finally, the equivalent plastic strain rate $\dot{\bar{\varepsilon}}^{\mathrm{p}}$ is specified as

$$\dot{\bar{\varepsilon}}^{\mathrm{p}} = f(\tilde{\sigma}, s) \tag{16}$$

and the evolution of the scalar state variable s (internal resistance to plastic deformation) is given by

$$\dot{s} = g(\tilde{\sigma}, s) \equiv h(\tilde{\sigma}, s) f(\tilde{\sigma}, s) \tag{17}$$

The functions $f(\tilde{\sigma}, s)$ and $h(\tilde{\sigma}, s)$ are experimentally determined for a particular material [27].

With the above constitutive equations, one can solve the weak form of the equilibrium equations (Equation (7)) to calculate the deformation and evolution of state induced by given applied loads or kinematic boundary conditions [28]. Contact constraints play an important role for metal forming processes [29, 30]. A brief presentation of the contact sub-problem is given next in order to set the notation for the development of the contact sensitivity algorithm.

2.2. *The contact sub-problem*

A schematic of the contact sub-problem is shown in Figure 1. The presentation is limited to plane-strain and axisymmetric problems and dies are considered to be rigid. The die $\mathscr{D}$ is parametrized using a parameter ξ and the die functions $\mathbf{y}(\xi) = (y_1(\xi), y_3(\xi)), 0 \leqslant \xi \leqslant 1$. A fixed right-handed basis $(\mathbf{e}_1, \mathbf{e}_2, \mathbf{e}_3)$ is defined, with $\mathbf{e}_2$ pointing into the plane of the paper. A convected basis $(\mathbf{r}, \mathbf{e}_2, \boldsymbol{\nu})$ is defined at each point (i.e. for each particular value of ξ). The tangent vector $\boldsymbol{\tau}_1$, and the unit tangent vector $\mathbf{r}$ are given as

$$\boldsymbol{\tau}_1 = \mathbf{y}_{,\xi} = \frac{\partial y_1}{\partial \xi}\mathbf{e}_1 + \frac{\partial y_3}{\partial \xi}\mathbf{e}_3, \quad \mathbf{r} = \frac{\boldsymbol{\tau}_1}{\|\boldsymbol{\tau}_1\|} \tag{18}$$

The die separates the space into admissible and inadmissible regions and the die is parametrized such that the normal vector $\boldsymbol{\nu}$ is pointing into the admissible region [29]. With this convention, the unit normal vector $\boldsymbol{\nu}$ points towards the body (i.e. $\boldsymbol{\nu} = -\mathbf{n}$, where $\mathbf{n}$ is the outward unit normal vector to the body). Figure 1 shows a schematic of the contact sub-problem and introduces the notation for the various contact parameters. The gap function g of any point $\mathbf{x}$ in space is defined as the shortest distance of that point from the die. Thus, we write

$$\bar{\mathbf{y}} - \mathbf{x} = g(\mathbf{x})\boldsymbol{\nu}(\bar{\mathbf{y}}) \tag{19}$$

where $\bar{\mathbf{y}} \in \mathscr{D}$ is the value of $\mathbf{y}$ that minimizes the norm, $\|\mathbf{x} - \mathbf{y}\|$. A unique value of the parameter $\bar{\xi}$ is associated with each $\bar{\mathbf{y}}$.

Following the work in Reference [29], the contact traction vector $\boldsymbol{\lambda}$ per unit reference area $\boldsymbol{\Gamma} \subset \partial\mathbf{B}_n$ is introduced and its components λ_{N} and λ_{T} are defined as follows:

$$\boldsymbol{\lambda} = \lambda_{\mathrm{N}}\boldsymbol{\nu} - \lambda_{\mathrm{T}}\boldsymbol{\tau}_1 \tag{20}$$

The impenetrability constraints can now be written as follows: For all $\mathbf{x}_n \in \boldsymbol{\Gamma}$, with $\mathbf{x}_{n+1} = \mathbf{x}_n + \mathbf{u}(\mathbf{x}_n)$,

$$\lambda_{\mathrm{N}} \geqslant 0, \quad g(\mathbf{x}_{n+1}) \leqslant 0, \quad \lambda_{\mathrm{N}} g(\mathbf{x}_{n+1}) = 0 \tag{21}$$

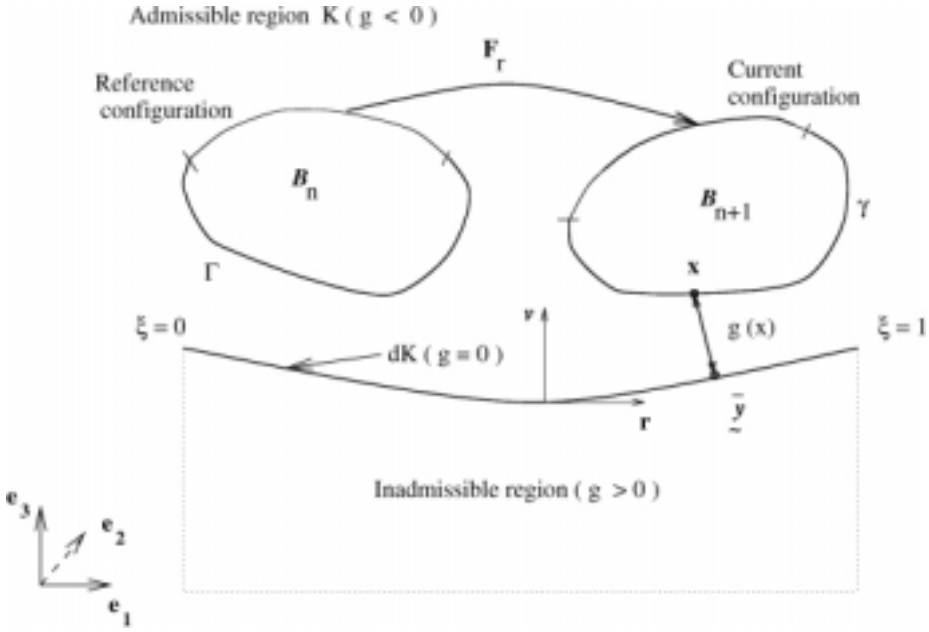

Figure 1. A schematic of the contact sub-problem showing the body configurations at times t_n and t_{n+1}, the definition of the gap function $g(\mathbf{x})$ and the admissible and inadmissible regions. $\boldsymbol{\Gamma}$ refers to the part of the boundary $\partial\mathbf{B}_n$ that could potentially come in contact.

The Coulomb friction law can be written as:

$$\begin{aligned} \boldsymbol{\lambda}_{\mathrm{T}} &= -\boldsymbol{\lambda} + \lambda_{\mathrm{N}}\mathbf{v} \\ \Upsilon := \|\boldsymbol{\lambda}_{\mathrm{T}}\| - \mu\lambda_{\mathrm{N}} &\leqslant 0 \\ \mathbf{v}_{\mathrm{T}} &= \chi\frac{\boldsymbol{\lambda}_{\mathrm{T}}}{\|\boldsymbol{\lambda}_{\mathrm{T}}\|} \\ \chi &\geqslant 0 \\ \chi\Upsilon &= 0 \end{aligned} \tag{22}$$

An augmented Lagrangian algorithm that enforces the above contact and friction constraints, is presented in the next section.

2.3. *Basic elements of a Lagrangian analysis*

In the updated Lagrangian FEM formulation, a sequence of incremental problems is defined from time t_n to t_{n+1}, $n = 0, 1, 2, \ldots$. Within each time increment, the deformation problem is further divided into three incremental sub-problems: (1) the constitutive problem, (2) the kinematic problem and (3) the contact problem.

In the constitutive incremental problem, one calculates $(\mathbf{T}_{n+1}, s_{n+1}, \bar{\mathbf{F}}^{\mathrm{p}}_{n+1})$ given the incremental deformation gradient $\mathbf{F}_{\mathrm{r}}$ from t_n to t_{n+1} (see Figure 1) and $(\mathbf{T}_n, s_n, \bar{\mathbf{F}}^{\mathrm{p}}_n)$. Constitutive integration techniques for such problems can be found in Reference [31]. In the present analysis the radial return mapping of Reference [26] is implemented.

In the kinematic problem, one calculates the incremental displacements from t_n to t_{n+1} given the triad $(\mathbf{T}, s, \bar{\mathbf{F}}^{\mathrm{p}})$ at t_{n+1}. A Newton–Raphson scheme is developed by linearizing the weak form of the equilibrium equation [28].

In the contact sub-problem, given the configuration $\mathbf{B}_{n+1}$, the die location and shape at t_{n+1}, as well as estimates of the contact tractions from a previous time step or a Newton iteration, one computes (updates) regions of contact as well as the contact traction components λ_{N} and λ_{T}.

The time integration of the contact sub-problem based on the augmented Lagrangian analysis of Laursen and Simo [29, 30], is briefly reviewed since it is essential for the presentation of the proposed sensitivity methodology. The time integration of the frictional constraint is achieved by the introduction of a trial state and a subsequent return map. In the algorithm below, k refers to the augmentation index and j refers to the Newton–Raphson iteration index. The terms G and G_{c} in the kinematic problem refer to the principle of virtual work and contributions from the internal work/non-contact related boundary terms and contact terms, respectively [28].

1. Initialization:

   $\lambda_{\mathrm{N}}^{(0)} = \langle \lambda_{\mathrm{N}_n} + \varepsilon_{\mathrm{N}} g(\mathbf{x}_{n+1}^{(0)}) \rangle$
   $\Delta\lambda_{\mathrm{T}}^{(0)} = 0$
   $k = 0$
2. Solve for the incremental displacement $\mathbf{u}^{(k)} = \mathbf{x}_{n+1}^{(k)} - \mathbf{x}_n$ which is the converged estimate of $\mathbf{u}_j^{(k)} = \mathbf{x}_{n+1,j}^{(k)} - \mathbf{x}_n$:

   $$\tilde{G}(\mathbf{u}_j^{(k)}, \tilde{\mathbf{u}}) = G(\mathbf{u}_j^{(k)}, \tilde{\mathbf{u}}) + G_{\mathrm{c}}(\mathbf{u}_j^{(k)}, \tilde{\mathbf{u}}) = 0$$

   Note: The above equation is non-linear and is solved iteratively (iteration j) [28]. A Newton–Raphson algorithm is used to solve this system and the computation of the linearized stiffness matrix and residual is dependent on the solution of the kinematic, constitutive and contact sub-problems. The solution of this non-linear equation predicts estimates of the body configuration $\mathbf{B}_{(n+1),j}^k$ at t_{n+1} and finally the converged solution $\mathbf{B}_{n+1}^k$.
   The contact traction $\boldsymbol{\lambda}_{j-1}^k$ used in the solution of the linearized principle of virtual work (based on the estimate $\mathbf{B}_{(n+1),j-1}^k$) is calculated as follows:

   Normal traction:

   $$\lambda_{\mathrm{N}} = \langle \lambda_{\mathrm{N}}^{(k)} + \varepsilon_{\mathrm{N}} g(\mathbf{x}_{(n+1),j-1}^{(k)}) \rangle$$

   Tangential traction:
   Compute trial state:

   $$\lambda_{\mathrm{T}}^{\mathrm{trial}} = \lambda_{\mathrm{T}_n} + \varepsilon_{\mathrm{T}}(\bar{\xi}_{(n+1),j-1}^{(k)} - \bar{\xi}_n) + \Delta\lambda_{\mathrm{T}}^{(k)}$$
   $$\Upsilon^{\mathrm{trial}} = \|\boldsymbol{\lambda}_{\mathrm{T}}^{\mathrm{trial}}\| - \mu\lambda_{\mathrm{N}}$$

   Radial return update:

   IF $(\Upsilon^{\mathrm{trial}} \leqslant 0)$
   THEN $\lambda_{\mathrm{T}} = \lambda_{\mathrm{T}}^{\mathrm{trial}}$ (stick)

ELSE (return map)

$$\lambda_{\mathrm{T}} = \mu\lambda_{\mathrm{N}} \frac{\lambda_{\mathrm{T}}^{\mathrm{trial}}}{\|\boldsymbol{\lambda}_{\mathrm{T}}^{\mathrm{trial}}\|} \text{ (slip)}$$

Complete contact traction description:

$$\boldsymbol{\lambda}_{j-1}^{k} = \lambda_{\mathrm{N}}\mathbf{v}(\bar{\mathbf{y}}) - \lambda_{\mathrm{T}}\boldsymbol{\tau}_1(\bar{\mathbf{y}})$$

3. Check for contact constraints satisfaction:
IF $g(\mathbf{x}_{n+1}^{(k)}) \leqslant \mathrm{TOLg}$ AND
$\|\bar{\xi}_{n+1}^{(k)} - \bar{\xi}_n\| \leqslant \mathrm{TOLf}\ \forall\, \mathbf{x}_n \in \boldsymbol{\Gamma}$ such that $\|\boldsymbol{\lambda}_{\mathrm{T}}\| < \mu\langle\lambda_{\mathrm{N}}^{(k)} + \varepsilon_{\mathrm{N}} g(\mathbf{x}_{n+1}^{(k)})\rangle$
THEN
CONVERGED (GOTO 4)
ELSE AUGMENT ($\forall\, \mathbf{x}_n \in \boldsymbol{\Gamma}$)
$\lambda_{\mathrm{N}}^{(k+1)} = \langle\lambda_{\mathrm{N}}^{(k)} + \varepsilon_{\mathrm{N}} g(\mathbf{x}_{n+1}^{(k)})\rangle$
$\lambda_{\mathrm{T}}^{\mathrm{trial}} = \lambda_{\mathrm{T}_n} + \varepsilon_{\mathrm{T}}(\bar{\xi}_{n+1}^{(k)} - \bar{\xi}_n) + \Delta\lambda_{\mathrm{T}}^{(k)}$
$\Upsilon^{\mathrm{trial}} = \|\boldsymbol{\lambda}_{\mathrm{T}}^{\mathrm{trial}}\| - \mu\lambda_{\mathrm{N}}^{(k+1)}$
IF ($\Upsilon^{\mathrm{trial}} \leqslant 0$)
THEN
$\Delta\lambda_{\mathrm{T}}^{(k+1)} = \Delta\lambda_{\mathrm{T}}^{(k)} + \varepsilon_{\mathrm{T}}\Delta\bar{\xi}^{(k)}$ (stick)
ELSE (return map)
$\Delta\lambda_{\mathrm{T}}^{(k+1)} = \mu\lambda_{\mathrm{N}}^{(k+1)} \frac{\lambda_{\mathrm{T}}^{\mathrm{trial}}}{\|\boldsymbol{\lambda}_{\mathrm{T}}^{\mathrm{trial}}\|} - \lambda_{\mathrm{T}_n}$ (slip)
ENDIF
$k = k + 1$
GOTO 2
ENDIF

4. Post-process operation:
Use the converged solution of the configuration $\mathbf{B}_{n+1}$ to update the triad $(\mathbf{T}, s, \bar{\mathbf{F}}^{\mathrm{p}})$ as well as the contact traction components $(\lambda_{\mathrm{N}}, \lambda_{\mathrm{T}})$ at time t_{n+1}.

The three sub-problems (constitutive, kinematic and contact) are solved in an iterative manner. More details on the implementation of these problems can be found in References [28, 32] where an object-oriented environment for finite deformation problems is discussed.

3. THE SENSITIVITY PROBLEM

3.1. Definition of sensitivity fields

A definition is given for the sensitivity of any field related to the direct problem (e.g. of the deformation gradient, stress, state variables, etc.) with respect to the die shape. The parameter $\boldsymbol{\beta}_p$ introduced below is either the die surface itself (i.e. $\boldsymbol{\beta}_p$ is a function) or a set of algebraic parameters that define the die surface in a finite dimensional space as discussed in Section 1. Before we proceed, it is mentioned that $\boldsymbol{\beta}_p$ can also represent any other non-shape related process

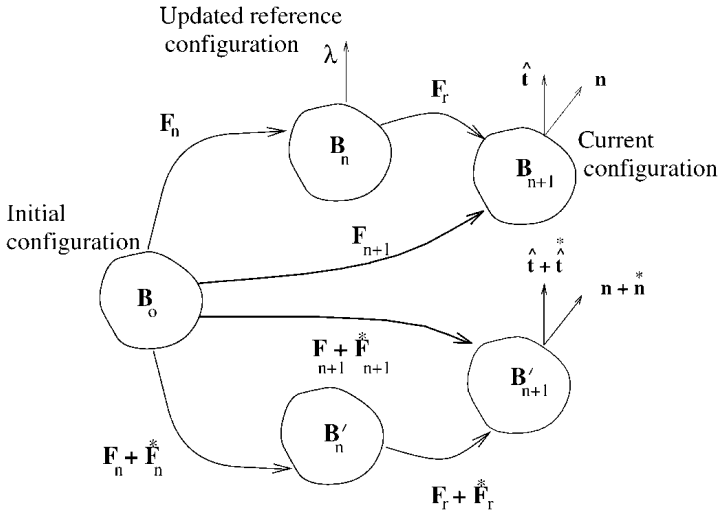

Figure 2. Schematic diagram of the deformation history of a workpiece corresponding to two dies defined by the design parameters $\boldsymbol{\beta}_p$ and $(\boldsymbol{\beta}_p + \Delta\boldsymbol{\beta}_p)$. Note that in the deformation process with a die $\boldsymbol{\beta}_p + \Delta\boldsymbol{\beta}_p$, the relative deformation gradient from t_n to t_{n+1} is easily shown to be $\mathbf{F}_{\mathrm{r}} + \overset{*}{\mathbf{F}}_{\mathrm{r}}$, where $\overset{*}{\mathbf{F}}_{\mathrm{r}} = (\overset{*}{\mathbf{F}}_{n+1} - \mathbf{F}_{\mathrm{r}}\,\overset{*}{\mathbf{F}}_n)\mathbf{F}_n^{-1}$.

parameter such as the ram or die speed, operating temperature, lubrication conditions as well as the initial material state. For preform design and related shape optimization problems, see References [25, 33]. For clarity of the presentation, unless otherwise stated, we only refer to sensitivities with respect to the die surface.

Let $\boldsymbol{\Phi}(\mathbf{X}, t; \boldsymbol{\beta}_p)$ be a Lagrangian field defined in the direct analysis for a given choice of design $\boldsymbol{\beta}_p$. The notation $\boldsymbol{\Phi}(\mathbf{X}, t; \boldsymbol{\beta}_p)$ implies that $\boldsymbol{\Phi}$ can be uniquely determined by solving the direct deformation problem for a particular set of boundary conditions resulting from a die defined by $\boldsymbol{\beta}_p$. Figure 2 shows the configurations of the body during a deformation process for two different but nearby sets of design parameters (i.e. two nearby dies).

We define the sensitivity $\overset{*}{\boldsymbol{\Phi}}(\mathbf{X}, t; \boldsymbol{\beta}_p, \Delta\boldsymbol{\beta}_p)$ of $\boldsymbol{\Phi}$ as the directional derivative (Gateaux differential) of $\boldsymbol{\Phi}$ with respect to $\boldsymbol{\beta}_p$ in the direction of $\Delta\boldsymbol{\beta}_p$, i.e.

$$\begin{aligned}\overset{*}{\boldsymbol{\Phi}}(\mathbf{X}, t; \boldsymbol{\beta}_p, \Delta\boldsymbol{\beta}_p) &= \frac{\mathrm{d}}{\mathrm{d}\lambda}\,[\boldsymbol{\Phi}(\mathbf{X}, t; \boldsymbol{\beta}_p + \lambda\Delta\boldsymbol{\beta}_p)]\big|_{\lambda=0} \\ &= \boldsymbol{\Phi}(\mathbf{X}, t; \boldsymbol{\beta}_p + \Delta\boldsymbol{\beta}_p) - \boldsymbol{\Phi}(\mathbf{X}, t; \boldsymbol{\beta}_p) + \mathrm{O}(\|\Delta\boldsymbol{\beta}_p\|^2)\end{aligned} \tag{23}$$

Based on the above definition, one can easily define temporal and spatial derivatives of sensitivity fields [24]. The sensitivity of Eulerian fields can be calculated by first transforming them to Lagrangian fields (via the mapping given by Equation (1)) and then applying the definition given in Equation (23).

3.2. The overall deformation sensitivity problem

Given the die design parameters $\boldsymbol{\beta}_p$ and with the remaining boundary and process conditions fixed, one can solve the direct deformation problem and calculate the material state, deformation and

stresses at each time step. On the other hand in the sensitivity problem, one is interested in computing the sensitivity history of the material state, deformation and stresses around a die $\boldsymbol{\beta}_p$ and with a die perturbation $\Delta\boldsymbol{\beta}_p$. In simple terms, the sensitivity of a given direct field tells us how much this field will change from its value obtained from the direct deformation problem solution obtained with a die $\boldsymbol{\beta}_p$ if the die is perturbed by an amount $\Delta\boldsymbol{\beta}_p$.

As in the direct analysis, the *incremental deformation sensitivity problem* (from time t_n to time t_{n+1}) is divided into three coupled sub-problems, the constitutive, kinematic and contact sensitivity sub-problems. In the *incremental constitutive sensitivity problem*, given the sensitivity fields at time t_n, $[\overset{*}{s}_n, \overset{*}{\mathbf{F}}_n]$, as well as the direct fields at time t_{n+1}, $[\mathbf{T}_{n+1}, s_{n+1}, \mathbf{F}_{n+1}, \bar{\mathbf{F}}^{\mathrm{p}}_{n+1}]$, one calculates the linear relations between each of the sensitivity fields $[\overset{*}{\mathbf{T}}_{n+1}, \overset{*}{s}_{n+1}, \overset{*}{\mathbf{F}}^{\mathrm{e}}_{n+1}]$ and $\overset{*}{\mathbf{F}}_{n+1}$. In the *incremental kinematic sensitivity problem*, given the direct problem solution at t_{n+1}, i.e. given $[\mathbf{T}_{n+1}, s_{n+1}, \mathbf{F}_{n+1}, \bar{\mathbf{F}}^{\mathrm{p}}_{n+1}]$, and with the given linear relations between $[\overset{*}{\mathbf{T}}_{n+1}, \overset{*}{s}_{n+1}, \overset{*}{\mathbf{F}}^{\mathrm{e}}_{n+1}]$ and $\overset{*}{\mathbf{F}}_{n+1}$, one calculates $\overset{*}{\mathbf{F}}_{n+1}$. In the *incremental contact sensitivity problem*, given the contact traction components λ_{N} and λ_{T} at time t_{n+1} as well as the identity of regions of sliding and sticking, one computes the linear relation between the sensitivities $\overset{*}{\lambda}_{\mathrm{N}}$ and $\overset{*}{\lambda}_{\mathrm{T}}$ at t_{n+1} and the sensitivity $\overset{*}{\mathbf{x}}$ of the contact boundary in the current configuration $\mathbf{B}_{n+1}$.

Remark 1. For simplification, it has been selected in the direct analysis to track and report the calculation of the triad $\mathbf{V}_{n+1} \equiv [\mathbf{T}_{n+1}, s_{n+1}, \bar{\mathbf{F}}^{\mathrm{p}}_{n+1}]$ and $\mathbf{F}_{n+1}$, whereas in the sensitivity analysis the duo $\overset{*}{\mathbf{W}}_{n+1} \equiv [\overset{*}{s}_{n+1}, \overset{*}{\mathbf{F}}^{\mathrm{e}}_{n+1}]$ and $\overset{*}{\mathbf{F}}_{n+1}$ are computed and reported. The selection in the sensitivity analysis of $\overset{*}{\mathbf{F}}^{\mathrm{e}}_{n+1}$ to define the sensitivity of the intermediate configuration instead of $\overset{*}{\bar{\mathbf{F}}}^{\mathrm{p}}_{n+1}$ is for convenience of the presentation since $\overset{*}{\mathbf{F}}^{\mathrm{e}}_{n+1}$ and $\overset{*}{\mathbf{F}}_{n+1}$ uniquely define $\overset{*}{\bar{\mathbf{F}}}^{\mathrm{p}}_{n+1}$ for given $\bar{\mathbf{F}}^{\mathrm{p}}_{n+1}$ and $\mathbf{F}_{n+1}$.

The three incremental sensitivity problems (constitutive, kinematic and contact) are linearly coupled and together provide a linear problem for the calculation of sensitivities of both the deformation and the material state at t_{n+1}. It should be noted that the corresponding sub-problems in the direct problem are non-linearly coupled and are solved in an iterative fashion [31].

3.2.1. The constitutive sensitivity problem. The incremental constitutive sensitivity problem is defined in Reference [24] and is briefly described here for clarity and completeness of the presentation. The present mathematical approach to this problem is similar to that of Reference [24], however, the implementation is quite different. The solution of the constitutive sensitivity problem follows the following steps:

Calculation of the linear relations between $\overset{*}{\bar{\mathbf{T}}}'_{n+1}$, $\overset{*}{\tilde{\sigma}}_{n+1}$ and $\overset{*}{\mathbf{F}}^{\mathrm{e}}_{n+1}$

By following the definitions of $\bar{\mathbf{T}}'$ (Equation (15)) and $\tilde{\sigma}$ (Equation (14)), the sensitivities $\overset{*}{\bar{\mathbf{T}}}'_{n+1}$ and $\overset{*}{\tilde{\sigma}}_{n+1}$ are obtained as follows:

$$\overset{*}{\bar{\mathbf{T}}}'_{n+1} = \overset{*}{\bar{\mathbf{T}}}_{n+1} - \frac{1}{3}\mathrm{tr}(\overset{*}{\bar{\mathbf{T}}}_{n+1})\mathbf{I} \tag{24}$$

and

$$\overset{*}{\tilde{\sigma}}_{n+1} = \frac{3}{2}\frac{\bar{\mathbf{T}}'_{n+1} \cdot \overset{*}{\bar{\mathbf{T}}}'_{n+1}}{\tilde{\sigma}_{n+1}} \tag{25}$$

By differentiating the hyperelastic law in Equation (8), $\overset{*}{\bar{\mathbf{T}}}_{n+1}$ is expressed as:

$$\overset{*}{\bar{\mathbf{T}}}_{n+1} = \mathscr{L}^{\mathrm{e}}[\overset{*}{\bar{\mathbf{E}}}^{\mathrm{e}}_{n+1}] \tag{26}$$

By employing the first Padé approximation of the logarithm of $\mathbf{U}^{\mathrm{e}}$ and taking the sensitivity, $\overset{*}{\bar{\mathbf{E}}}^{\mathrm{e}}_{n+1}$ can be written as

$$\overset{*}{\bar{\mathbf{E}}}^{\mathrm{e}}_{n+1} = 4(\mathbf{U}^{\mathrm{e}}_{n+1} + \mathbf{I})^{-1}\overset{*}{\mathbf{U}}^{\mathrm{e}}_{n+1}(\mathbf{U}^{\mathrm{e}}_{n+1} + \mathbf{I})^{-1} \tag{27}$$

where

$$\overset{*}{\mathbf{U}}^{\mathrm{e}}_{n+1} = \mathrm{sym}(\mathbf{U}^{\mathrm{e}-1}_{n+1}\mathrm{sym}(\mathbf{F}^{\mathrm{e}\mathrm{T}}_{n+1}\overset{*}{\mathbf{F}}^{\mathrm{e}}_{n+1})) \tag{28}$$

Equations (24)–(28) and the linear transformation equations presented in Appendix A of Reference [24] can easily be combined to provide the linear relations between $\overset{*}{\bar{\mathbf{T}}}'_{n+1}$ and $\overset{*}{\mathbf{F}}^{\mathrm{e}}_{n+1}$ as well as $\overset{*}{\tilde{\sigma}}_{n+1}$ and $\overset{*}{\mathbf{F}}^{\mathrm{e}}_{n+1}$.

Calculation of the linear relation between $\overset{*}{\bar{\mathbf{F}}}^{\mathrm{p}}_{n+1}[\bar{\mathbf{F}}^{\mathrm{p}}]^{-1}_{n+1}$ and $\overset{*}{\mathbf{F}}^{\mathrm{e}}_{n+1}$
According to the definition of $\bar{\mathbf{D}}^{\mathrm{p}}$ (Equation (12)), one can write the following:

$$\begin{aligned}\overset{*}{\bar{\mathbf{D}}}^{\mathrm{p}} &= \frac{\mathrm{d}}{\mathrm{d}t}(\overset{*}{\bar{\mathbf{F}}}^{\mathrm{p}})[\bar{\mathbf{F}}^{\mathrm{p}}]^{-1} - \bar{\mathbf{D}}^{\mathrm{p}}\overset{*}{\bar{\mathbf{F}}}^{\mathrm{p}}[\bar{\mathbf{F}}^{\mathrm{p}}]^{-1} \\ &= \frac{\mathrm{d}}{\mathrm{d}t}(\overset{*}{\bar{\mathbf{F}}}^{\mathrm{p}}[\bar{\mathbf{F}}^{\mathrm{p}}]^{-1}) + \overset{*}{\bar{\mathbf{F}}}^{\mathrm{p}}[\bar{\mathbf{F}}^{\mathrm{p}}]^{-1}\bar{\mathbf{D}}^{\mathrm{p}} - \bar{\mathbf{D}}^{\mathrm{p}}\overset{*}{\bar{\mathbf{F}}}^{\mathrm{p}}[\bar{\mathbf{F}}^{\mathrm{p}}]^{-1}\end{aligned} \tag{29}$$

We employ an Euler-backward integration scheme over (t_n, t_{n+1}) to integrate Equation (29) and express the above equation as follows:

$$\frac{\mathrm{d}}{\mathrm{d}t}(\overset{*}{\bar{\mathbf{F}}}^{\mathrm{p}}[\bar{\mathbf{F}}^{\mathrm{p}}]^{-1}) + \overset{*}{\bar{\mathbf{F}}}^{\mathrm{p}}[\bar{\mathbf{F}}^{\mathrm{p}}]^{-1}\bar{\mathbf{D}}^{\mathrm{p}}_{n+1} - \bar{\mathbf{D}}^{\mathrm{p}}_{n+1}\overset{*}{\bar{\mathbf{F}}}^{\mathrm{p}}[\bar{\mathbf{F}}^{\mathrm{p}}]^{-1} = \overset{*}{\bar{\mathbf{D}}}^{\mathrm{p}}_{n+1}$$

Pre-multiplication of the above equation by $\exp(-t\,\bar{\mathbf{D}}^{\mathrm{p}}_{n+1})$, post-multiplication by $\exp(t\,\bar{\mathbf{D}}^{\mathrm{p}}_{n+1})$ and integration of the resulting equation, leads to the following:

$$\overset{*}{\bar{\mathbf{F}}}^{\mathrm{p}}_{n+1}[\bar{\mathbf{F}}^{\mathrm{p}}]^{-1}_{n+1} = \Delta\bar{\mathbf{F}}^{\mathrm{p}}\overset{*}{\bar{\mathbf{F}}}^{\mathrm{p}}_{n}[\bar{\mathbf{F}}^{\mathrm{p}}]^{-1}_{n}(\Delta\bar{\mathbf{F}}^{\mathrm{p}})^{-1} + \Delta t\,\overset{*}{\bar{\mathbf{D}}}^{\mathrm{p}}_{n+1} \tag{30}$$

where from the constitutive sub-problem of the direct problem [26],

$$\Delta\bar{\mathbf{F}}^{\mathrm{p}} = \bar{\mathbf{F}}^{\mathrm{p}}_{n+1}[\bar{\mathbf{F}}^{\mathrm{p}}]^{-1}_{n} = \exp(\Delta t\,\bar{\mathbf{D}}^{\mathrm{p}}_{n+1}) \tag{31}$$

with $\Delta t = t_{n+1} - t_n$. From Equation (12), one can derive the following:

$$\overset{*}{\bar{\mathbf{D}}}^{\mathrm{p}}_{n+1} = \frac{3}{2}\,\frac{f_{n+1}}{\tilde{\sigma}_{n+1}}\overset{*}{\bar{\mathbf{T}}}'_{n+1} + \frac{3}{2}\left(\frac{\tilde{\sigma}_{n+1}(f_{\tilde{\sigma}})_{n+1} - f_{n+1}}{\tilde{\sigma}^2_{n+1}}\overset{*}{\tilde{\sigma}}_{n+1} + \frac{(f_s)_{n+1}}{\tilde{\sigma}_{n+1}}\overset{*}{s}_{n+1}\right)\bar{\mathbf{T}}'_{n+1} \tag{32}$$

where from Equation (17), $\overset{*}{s}$ is obtained from

$$\frac{\mathrm{d}}{\mathrm{d}t}(\overset{*}{s}) = g_s \overset{*}{s} + g_{\tilde{\sigma}} \overset{*}{\tilde{\sigma}} \tag{33}$$

The subscripts to the functions $f(\tilde{\sigma}, s)$ and $g(\tilde{\sigma}, s)$ are used to denote partial derivatives with respect to their arguments. An Euler-backward integration of Equation (33) results in the following:

$$\overset{*}{s}_{n+1} = \overset{*}{s}_n \frac{1}{1 - \Delta t(g_s)_{n+1}} + \frac{(g_{\tilde{\sigma}})_{n+1}\Delta t}{1 - \Delta t(g_s)_{n+1}} \overset{*}{\tilde{\sigma}}_{n+1} \tag{34}$$

Substitution of Equations (32) and (34) in Equation (30) results in

$$\overset{*}{\bar{\mathbf{F}}}{}^{\mathrm{p}}_{n+1}[\bar{\mathbf{F}}^{\mathrm{p}}]^{-1}_{n+1} = \mathbf{C}_{n+1} + a_{n+1}\overset{*}{\bar{\mathbf{T}}}{}'_{n+1} + b_{n+1}\overset{*}{\tilde{\sigma}}_{n+1}\bar{\mathbf{T}}'_{n+1} \tag{35}$$

where

$$\mathbf{C}_{n+1} = \Delta\bar{\mathbf{F}}^{\mathrm{p}}(\overset{*}{\bar{\mathbf{F}}}{}^{\mathrm{p}}_n[\bar{\mathbf{F}}^{\mathrm{p}}]^{-1}_n)(\Delta\bar{\mathbf{F}}^{\mathrm{p}})^{-1} + \frac{3(f_s)_{n+1}}{2\,\tilde{\sigma}_{n+1}(1 - \Delta t(g_s)_{n+1})} \overset{*}{s}_n \,\Delta t\, \bar{\mathbf{T}}'_{n+1} \tag{36}$$

$$a_{n+1} = \frac{3 f_{n+1}\Delta t}{2\,\tilde{\sigma}_{n+1}} \tag{37}$$

$$b_{n+1} = \frac{3}{2}\left\{ \frac{\tilde{\sigma}_{n+1}(f_{\tilde{\sigma}})_{n+1} - f_{n+1}}{\tilde{\sigma}^2_{n+1}} + \frac{(f_s)_{n+1}(g_{\tilde{\sigma}})_{n+1}\Delta t}{\tilde{\sigma}_{n+1}(1 - \Delta t(g_s)_{n+1})} \right\} \Delta t \tag{38}$$

The sensitivity fields $\overset{*}{\bar{\mathbf{T}}}{}'_{n+1}$ and $\overset{*}{\tilde{\sigma}}_{n+1}$ were written earlier as linear functions of $\overset{*}{\mathbf{F}}{}^{\mathrm{e}}_{n+1}$ (see Equations (24)–(28)). As a result, Equation (35) provides the linear relation between $\overset{*}{\bar{\mathbf{F}}}{}^{\mathrm{p}}_{n+1}[\bar{\mathbf{F}}^{\mathrm{p}}]^{-1}_{n+1}$ and $\overset{*}{\mathbf{F}}{}^{\mathrm{e}}_{n+1}$.

Calculation of the linear relation between $\overset{*}{\mathbf{F}}{}^{\mathrm{e}}_{n+1}$ and $\overset{*}{\mathbf{F}}_{n+1}$

Starting from the multiplicative decomposition of the deformation gradient, one can write

$$\overset{*}{\mathbf{F}}_{n+1} = \overset{*}{\mathbf{F}}{}^{\mathrm{e}}_{n+1}\bar{\mathbf{F}}^{\mathrm{p}}_{n+1} + \mathbf{F}^{\mathrm{e}}_{n+1}\overset{*}{\bar{\mathbf{F}}}{}^{\mathrm{p}}_{n+1} \tag{39}$$

Hence,

$$[\mathbf{F}^{\mathrm{e}}]^{-1}_{n+1}(\overset{*}{\mathbf{F}}_{n+1}[\mathbf{F}]^{-1}_{n+1})\mathbf{F}^{\mathrm{e}}_{n+1} = [\mathbf{F}^{\mathrm{e}}]^{-1}_{n+1}\overset{*}{\mathbf{F}}{}^{\mathrm{e}}_{n+1} + \overset{*}{\bar{\mathbf{F}}}{}^{\mathrm{p}}_{n+1}[\bar{\mathbf{F}}^{\mathrm{p}}]^{-1}_{n+1} \tag{40}$$

As has already been shown, $\overset{*}{\bar{\mathbf{T}}}{}'_{n+1}$ and $\overset{*}{\tilde{\sigma}}_{n+1}$ linearly depend on $\overset{*}{\mathbf{F}}{}^{\mathrm{e}}_{n+1}$. Therefore substitution of Equation (35) in Equation (40) results in a linear relation between $\overset{*}{\mathbf{F}}{}^{\mathrm{e}}_{n+1}$ and $\overset{*}{\mathbf{F}}_{n+1}$

$$[\mathbf{F}^{\mathrm{e}}]^{-1}_{n+1}(\overset{*}{\mathbf{F}}_{n+1}[\mathbf{F}]^{-1}_{n+1})\mathbf{F}^{\mathrm{e}}_{n+1} - \mathbf{C}_{n+1} = [\mathbf{F}^{\mathrm{e}}]^{-1}_{n+1}\overset{*}{\mathbf{F}}{}^{\mathrm{e}}_{n+1} + a_{n+1}\overset{*}{\bar{\mathbf{T}}}{}'_{n+1} + b_{n+1}\overset{*}{\tilde{\sigma}}_{n+1}\bar{\mathbf{T}}'_{n+1} \tag{41}$$

Using the simplifications of Appendix A and the linear transformation equations discussed in the Appendix of Reference [24], one can write the following:

$$\overset{*}{\mathbf{F}}{}^{\mathrm{e}}_{n+1} = \mathscr{A}(\mathbf{V}_{n+1})[\overset{*}{\mathbf{F}}_{n+1}] + \mathbf{A}(\mathbf{V}_{n+1}, \overset{*}{\mathbf{W}}_n) \tag{42}$$

where $\mathbf{A}$ is a second-order tensor function and $\mathscr{A}$ a fourth-order tensor function. $\mathbf{A}$ and $\mathscr{A}$ depend upon the direct fields $\mathbf{V}_{n+1} \equiv (\mathbf{T}_{n+1}, s_{n+1}, \bar{\mathbf{F}}^{\mathrm{p}}_{n+1})$ calculated at time t_{n+1} and the sensitivity fields $\overset{*}{\mathbf{W}}_n \equiv (\overset{*}{s}_n, \overset{*}{\mathbf{F}}{}^{\mathrm{e}}_n)$ calculated at time t_n.

Calculation of the linear relation between $\overset{*}{\mathbf{T}}_{n+1}$ and $\overset{*}{\mathbf{F}}{}^{\mathrm{e}}_{n+1}$ Linearizations similar to the ones performed in the direct analysis as part of the calculation of the tangent stiffness, are used here to calculate the sensitivity of the Cauchy stress. Following References [24, 26], one can express $\overset{*}{\mathbf{T}}$ as

$$\overset{*}{\mathbf{T}}_{n+1} = (\det \mathbf{U}^{\mathrm{e}}_{n+1})^{-1}\, \mathbf{R}^{\mathrm{e}}_{n+1}\, \overset{*}{\bar{\mathbf{T}}}_{n+1} \mathbf{R}^{\mathrm{e}\mathrm{T}}_{n+1} - \mathrm{tr}(\overset{*}{\bar{\mathbf{E}}}{}^{\mathrm{e}}_{n+1})\mathbf{T}_{n+1} + 2\mathrm{sym}(\overset{*}{\mathbf{R}}{}^{\mathrm{e}}_{n+1} \mathbf{R}^{\mathrm{e}\mathrm{T}}_{n+1} \mathbf{T}_{n+1}) \tag{43}$$

where

$$\overset{*}{\mathbf{R}}{}^{\mathrm{e}}_{n+1}[\mathbf{R}^{\mathrm{e}}]^{\mathrm{T}}_{n+1} = \overset{*}{\mathbf{F}}{}^{\mathrm{e}}_{n+1}[\mathbf{F}^{\mathrm{e}}]^{-1}_{n+1} - \mathbf{R}^{\mathrm{e}}_{n+1} \overset{*}{\mathbf{U}}{}^{\mathrm{e}}_{n+1}[\mathbf{U}^{\mathrm{e}}]^{-1}_{n+1}[\mathbf{R}^{\mathrm{e}}]^{\mathrm{T}}_{n+1} \tag{44}$$

Expressions for $\overset{*}{\bar{\mathbf{E}}}{}^{\mathrm{e}}_{n+1}$ and $\overset{*}{\mathbf{U}}{}^{\mathrm{e}}_{n+1}$ in terms of $\overset{*}{\mathbf{F}}{}^{\mathrm{e}}_{n+1}$ are given in Equations (27) and (28), respectively. The calculation of $\overset{*}{\bar{\mathbf{T}}}_{n+1}$ in terms of $\overset{*}{\mathbf{F}}{}^{\mathrm{e}}_{n+1}$ was reported above (Equations (26)–(28)).

3.2.2. The kinematic sensitivity problem. To calculate the sensitivity field $\overset{*}{\mathbf{F}}$, one needs to consider the sensitivity of the equilibrium Equation (5) in conjunction with a set of boundary conditions for this kinematic problem. In the following, a principle of virtual work like equation is developed to obtain $\overset{*}{\mathbf{F}}$. The non-contact related sensitivity boundary conditions are treated in this section, whereas the contact sensitivity problem is addressed in the next section. To simplify the notation, we omit the subscript $(n+1)$ for tensor variables that refer to time t_{n+1}.

The directional derivative of the equilibrium equations (Equation (5)) results in the following:

$$\nabla \cdot \overset{*}{\mathbf{P}} + \overset{*}{\mathbf{f}} = \mathbf{0} \quad \forall \mathbf{X} \in \mathbf{B}_0 \quad \text{and} \quad \forall t \in [0, t_f] \tag{45}$$

Based on the definition of $\mathbf{P}$ from Equation (6), $\overset{*}{\mathbf{P}}$ is calculated as

$$\overset{*}{\mathbf{P}} = \det \mathbf{F}[\mathrm{tr}(\overset{*}{\mathbf{F}}\, \mathbf{F}^{-1})\mathbf{T} + \overset{*}{\mathbf{T}} - \mathbf{T}(\overset{*}{\mathbf{F}}\, \mathbf{F}^{-1})^{\mathrm{T}}]\, \mathbf{F}^{-\mathrm{T}} \tag{46}$$

In the above equation, $\overset{*}{\mathbf{T}}$ is given by Equation (43). Suppose that the gravity is the only body force acting on the body. Let ρ_0 be the constant density of the body in the reference configuration and let $\mathbf{g}$ be the gravity constant. The body force density in the current configuration is given by

$$\mathbf{b} = \rho \mathbf{g} = \frac{\rho_0}{\det \mathbf{F}} \mathbf{g}$$

Hence, $\mathbf{f} = \rho_0 \mathbf{g}$, and therefore,

$$\overset{*}{\mathbf{f}} = \mathbf{0} \tag{47}$$

A variational form of the kinematic sensitivity problem can now be posed as the calculation of $\overset{*}{\mathbf{x}}(\mathbf{X}, t)$ such that

$$\int_{\mathbf{B}_0} (\nabla \cdot \overset{*}{\mathbf{P}}) \cdot \tilde{\mathbf{u}}(\mathbf{X}) \, \mathrm{d}V = 0 \tag{48}$$

where $\tilde{\mathbf{u}}(\mathbf{X})$ is a kinematically admissible sensitivity displacement field expressed over the reference configuration. With integration by parts, Equation (48) results in

$$\int_{\mathbf{B}_0} \overset{*}{\mathbf{P}} \cdot \frac{\partial \tilde{\mathbf{u}}}{\partial \mathbf{X}} \, \mathrm{d}V_0 = \int_{\partial \mathbf{B}_0} \overset{*}{\mathbf{P}} \mathbf{m} \cdot \tilde{\mathbf{u}} \, \mathrm{d}A_0 \tag{49}$$

where $\mathbf{m}$ is the unit outward normal at $\mathbf{X} \in \partial \mathbf{B}_0$. The reference configuration is not affected by the change in the die surface, therefore $\overset{*}{\mathbf{m}} = 0$. Transforming the term in the right-hand side of Equation (49), to the current configuration (where $\mathbf{n}$ is the corresponding unit normal vector) and substituting the expression for $\overset{*}{\mathbf{P}}$ from Equation (46), one can obtain,

$$\int_{\partial \mathbf{B}_0} \overset{*}{\mathbf{P}} \mathbf{m} \cdot \tilde{\mathbf{u}} \, \mathrm{d}A_0 = \int_{\partial \mathbf{B}_{n+1}} \{\mathrm{tr}(\overset{*}{\mathbf{F}} \mathbf{F}^{-1}) \mathbf{T} + \overset{*}{\mathbf{T}} - \mathbf{T}(\overset{*}{\mathbf{F}} \mathbf{F}^{-1})^{\mathrm{T}}\} \mathbf{n} \cdot \tilde{\mathbf{u}} \, \mathrm{d}A_{n+1} \tag{50}$$

The normal vector $\mathbf{n}$ in the current configuration can be expressed in terms of the deformation gradient field and the normal vector $\mathbf{m}$ as follows:

$$\mathbf{n} = \mathbf{F}^{-\mathrm{T}} \mathbf{m} / \| \mathbf{F}^{-\mathrm{T}} \mathbf{m} \| \tag{51}$$

Applying the sensitivity operator to the above equation and after some simplifications, one can show that

$$\overset{*}{\mathbf{n}} = \{(\overset{*}{\mathbf{F}} \mathbf{F}^{-1}) \cdot \mathbf{n} \otimes \mathbf{n}\} \mathbf{n} - (\overset{*}{\mathbf{F}} \mathbf{F}^{-1})^{\mathrm{T}} \mathbf{n} \tag{52}$$

Using the above equation, the sensitivity of the traction vector $\hat{\mathbf{t}} = \mathbf{T}\mathbf{n}$ (per unit current area) can be written as follows:

$$\overset{*}{\hat{\mathbf{t}}} = \{(\overset{*}{\mathbf{F}} \mathbf{F}^{-1}) \cdot \mathbf{n} \otimes \mathbf{n}\} \hat{\mathbf{t}} + \overset{*}{\mathbf{T}} \mathbf{n} - \mathbf{T}(\overset{*}{\mathbf{F}} \mathbf{F}^{-1})^{\mathrm{T}} \mathbf{n} \tag{53}$$

Equations (49), (50) and (53) finally lead to the following weak sensitivity problem: *Calculate* $\overset{*}{\mathbf{x}}(\mathbf{X}, t)$ *such that*

$$\int_{\mathbf{B}_0} \overset{*}{\mathbf{P}} \cdot \frac{\partial \tilde{\mathbf{u}}}{\partial \mathbf{X}} \, \mathrm{d}V_0 = \int_{\partial \mathbf{B}_{n+1}} \{(\overset{*}{\mathbf{F}} \mathbf{F}^{-1}) \cdot (\mathbf{I} - \mathbf{n} \otimes \mathbf{n})\} \hat{\mathbf{t}} \cdot \tilde{\mathbf{u}} \, \mathrm{d}A_{n+1} + \int_{\partial \mathbf{B}_{n+1}} \overset{*}{\hat{\mathbf{t}}} \cdot \tilde{\mathbf{u}} \, \mathrm{d}A_{n+1} \tag{54}$$

for every admissible test function $\tilde{\mathbf{u}}$.

In the direct contact analysis presented in Sections 2.2 and 2.3, the contact traction $\boldsymbol{\lambda}$ per unit reference area $\boldsymbol{\Gamma}$ was introduced. The contact traction vectors $\hat{\mathbf{t}}$ and $\boldsymbol{\lambda}$ are related as follows:

$$\hat{\mathbf{t}} = \boldsymbol{\lambda} \, \| \mathbf{F}_{\mathrm{r}}^{\mathrm{T}} \mathbf{n} \| / J_{\mathrm{r}} \tag{55}$$

where $\mathbf{F}_{\mathrm{r}} = \mathbf{F}\mathbf{F}_n^{-1}$ is the relative deformation gradient and $J_{\mathrm{r}} = \det \mathbf{F}_{\mathrm{r}}$. Using the fact that $\|\mathbf{F}_{\mathrm{r}}^{\mathrm{T}}\mathbf{n}\|/J_{\mathrm{r}} = \dfrac{\mathrm{d}A_n}{\mathrm{d}A_{n+1}}$, the first term in the right-hand side of Equation (54) can be expressed as

$$\int_{\partial\mathbf{B}_{n+1}} \{(\overset{*}{\mathbf{F}}\,\mathbf{F}^{-1}) \cdot (\mathbf{I} - \mathbf{n}\otimes\mathbf{n})\}\,\hat{\mathbf{t}}\cdot\tilde{\mathbf{u}}\,\mathrm{d}A_{n+1} = \int_{\partial\mathbf{B}_n} \{(\overset{*}{\mathbf{F}}\,\mathbf{F}^{-1}) \cdot (\mathbf{I} - \mathbf{n}\otimes\mathbf{n})\}\boldsymbol{\lambda}\cdot\tilde{\mathbf{u}}\,\mathrm{d}A_n \tag{56}$$

The sensitivity of the contact traction vector $\hat{\mathbf{t}}$ can be computed as

$$\overset{*}{\hat{\mathbf{t}}} = \overset{*}{\boldsymbol{\lambda}}\frac{\|\mathbf{F}_{\mathrm{r}}^{\mathrm{T}}\mathbf{n}\|}{J_{\mathrm{r}}} + \frac{\boldsymbol{\lambda}}{J_{\mathrm{r}}}\frac{\overset{*}{}}{\|\mathbf{F}_{\mathrm{r}}^{\mathrm{T}}\mathbf{n}\|} - \frac{\boldsymbol{\lambda}\|\mathbf{F}_{\mathrm{r}}^{\mathrm{T}}\mathbf{n}\|}{J_{\mathrm{r}}^2}\frac{\overset{*}{}}{\det\mathbf{F}_{\mathrm{r}}} \tag{57}$$

Equation (57) can be used to modify the right-hand side of Equation (54) as follows:

$$\int_{\partial\mathbf{B}_{n+1}} \overset{*}{\hat{\mathbf{t}}}\cdot\tilde{\mathbf{u}}\,\mathrm{d}A_{n+1} = \int_{\partial\mathbf{B}_{n+1}} \left(\overset{*}{\boldsymbol{\lambda}}\frac{\|\mathbf{F}_{\mathrm{r}}^{\mathrm{T}}\mathbf{n}\|}{J_{\mathrm{r}}} + \frac{\boldsymbol{\lambda}}{J_{\mathrm{r}}}\frac{\overset{*}{}}{\|\mathbf{F}_{\mathrm{r}}^{\mathrm{T}}\mathbf{n}\|} - \frac{\boldsymbol{\lambda}\|\mathbf{F}_{\mathrm{r}}^{\mathrm{T}}\mathbf{n}\|}{J_{\mathrm{r}}^2}\frac{\overset{*}{}}{\det\mathbf{F}_{\mathrm{r}}}\right)\cdot\tilde{\mathbf{u}}\,\mathrm{d}A_{n+1} \tag{58}$$

The first term in the right-hand side of the above equation simplifies as

$$\int_{\partial\mathbf{B}_{n+1}} \overset{*}{\boldsymbol{\lambda}}\frac{\|\mathbf{F}_{\mathrm{r}}^{\mathrm{T}}\mathbf{n}\|}{J_{\mathrm{r}}}\cdot\tilde{\mathbf{u}}\,\mathrm{d}A_{n+1} = \int_{\partial\mathbf{B}_n} \overset{*}{\boldsymbol{\lambda}}\cdot\tilde{\mathbf{u}}\,\mathrm{d}A_n \tag{59}$$

The computation of the sensitivity of the contact traction vector $\overset{*}{\boldsymbol{\lambda}}$ is derived in the next section.

The following expression can be shown to hold:

$$\frac{\overset{*}{}}{\|\mathbf{F}_{\mathrm{r}}^{\mathrm{T}}\mathbf{n}\|} = [(\mathbf{F}_{\mathrm{r}}\mathbf{F}_{\mathrm{r}}^{\mathrm{T}})\cdot(\overset{*}{\mathbf{n}}\otimes\mathbf{n}) + (\overset{*}{\mathbf{F}}_{\mathrm{r}}\,\mathbf{F}_{\mathrm{r}}^{\mathrm{T}})\cdot(\mathbf{n}\otimes\mathbf{n})]\frac{1}{\|\mathbf{F}_{\mathrm{r}}^{\mathrm{T}}\mathbf{n}\|} \tag{60}$$

where the sensitivity of the relative deformation gradient is expressed as

$$\overset{*}{\mathbf{F}}_{\mathrm{r}} = (\overset{*}{\mathbf{F}} - \mathbf{F}_{\mathrm{r}}\overset{*}{\mathbf{F}}_n)\mathbf{F}_n^{-1} \tag{61}$$

The sensitivity of J_{r} is computed as

$$\frac{\overset{*}{}}{\det\mathbf{F}_{\mathrm{r}}} = J_{\mathrm{r}}\,\mathrm{tr}(\overset{*}{\mathbf{F}}\,\mathbf{F}^{-1}) - J_{\mathrm{r}}\,\mathrm{tr}(\mathbf{F}_{\mathrm{r}}\overset{*}{\mathbf{F}}_n\,\mathbf{F}^{-1}) \tag{62}$$

Equations (60) and (62) can be used to evaluate the second and third terms in the right-hand side of Equation (58). One can thus pose the weak kinematic sensitivity problem as follows:

Calculate $\overset{*}{\mathbf{x}}(\mathbf{X},t)$ *such that*

$$\int_{\mathbf{B}_0} \overset{*}{\mathbf{P}}\cdot\frac{\partial\tilde{\mathbf{u}}}{\partial\mathbf{X}}\,\mathrm{d}V_0 = \int_{\partial\mathbf{B}_n} \overset{*}{\boldsymbol{\lambda}}\cdot\tilde{\mathbf{u}}\,\mathrm{d}A_n + \int_{\partial\mathbf{B}_n} \mathrm{tr}[\mathbf{F}_{\mathrm{r}}\overset{*}{\mathbf{F}}_n\,\mathbf{F}^{-1}]\boldsymbol{\lambda}\cdot\tilde{\mathbf{u}}\,\mathrm{d}A_n$$
$$- \int_{\partial\mathbf{B}_n}\left[\frac{\mathbf{F}_{\mathrm{r}}\overset{*}{\mathbf{F}}_n\,\mathbf{F}_n^{-1}\mathbf{F}_{\mathrm{r}}^{\mathrm{T}}}{\|\mathbf{F}_{\mathrm{r}}^{\mathrm{T}}\mathbf{n}\|^2}\right]\cdot(\mathbf{n}\otimes\mathbf{n})\boldsymbol{\lambda}\cdot\tilde{\mathbf{u}}\,\mathrm{d}A_n \tag{63}$$

In the above equation, the integrations over the boundary $\partial\mathbf{B}_n$ are non-zero only on its subset $\boldsymbol{\Gamma}$ where contact occurs.

Remark 2. In using a finite element method to solve the above kinematic sensitivity problem for $\overset{*}{\mathbf{x}}$, one can notice that the term on the left-hand side of Equation (63) contributes to both the stiffness matrix and the force vector. Considering the right-hand side of the equation above, we remark that its first term contributes to both the stiffness matrix and the force vector (see Section 3.3), whereas its second and third terms contribute only to the force vector. In the present continuum sensitivity analysis, the stiffness matrix for the sensitivity problem is *not* the same as the linearized tangent stiffness used in the direct kinematic analysis, even though the relation of $\mathrm{d}\mathbf{P}$ with $\mathrm{d}\mathbf{F}$ and $\overset{*}{\mathbf{P}}$ with $\overset{*}{\mathbf{F}}$, respectively, look identical. This becomes apparent after noticing that $\overset{*}{\mathbf{P}}$ depends on $\overset{*}{\mathbf{T}}$ (Equation (46)) and through the solution of the constitutive sensitivity problem $\overset{*}{\mathbf{T}}$ depends upon the history of the sensitivities of the material state and $\mathbf{F}^{\mathrm{e}}$ (Equations (42) and (43)). Such dependencies are characteristic of the sensitivity problem and are of no relevance to the direct analysis.

3.2.3. Initial conditions and non-contact boundary sensitivity conditions. The following set of initial conditions are used in the direct analysis:

$$\mathbf{T}(\mathbf{X},0)=\mathbf{0}, \quad s(\mathbf{X},0)=s_0 \tag{64}$$

The corresponding initial conditions for the sensitivity problem are the following:

$$\overset{*}{\mathbf{T}}(\mathbf{X},0)=\mathbf{0}, \quad \overset{*}{s}(\mathbf{X},0)=0 \tag{65}$$

For calculating sensitivities with respect to the initial state or stresses, one should appropriately modify these equations.

The boundary conditions for the die sensitivity problem are derived from the corresponding boundary conditions of the direct analysis. Some typical non-contact related cases are examined below. The boundary traction is zero on a free boundary. The corresponding boundary condition for the sensitivity problem is written as follows:

$$\overset{*}{\hat{\mathbf{t}}}=\mathbf{0} \tag{66}$$

On the part of the boundary with prescribed displacement or velocity, e.g.

$$\mathbf{x}(\mathbf{X},t)=\tilde{\mathbf{x}}(\mathbf{X},t) \tag{67}$$

where $\tilde{\mathbf{x}}(\mathbf{X},t)$ is a known function, the corresponding kinematic sensitivity condition is

$$\overset{*}{\mathbf{x}}(\mathbf{X},t)=\mathbf{0} \tag{68}$$

The equation above should be modified if the objective is to calculate sensitivity fields with respect to design variables related to $\tilde{\mathbf{x}}(\mathbf{X},t)$ (for example when the ram speed is the design variable).

3.3. The contact sensitivity problem

As a result of the non-smooth nature of the contact/friction conditions, the calculation of the sensitivity of contact traction components is a non-trivial task. Non-smooth contact/frictional behaviour

result from the variation of the normal traction component at impending contact and from the variation of tangential traction component at the stick-slip transition. To allow for the differentiability of the direct contact/frictional conditions (see Section 2.3), the following regularizing assumptions are made:

(1) Contact sensitivity assumption: A material particle that lies in the admissible (inadmissible, respectively) region at time t for a particular deformation problem also lies in the admissible (inadmissible, respectively) region for a nearby deformation problem (e.g. obtained after an infinitesimal perturbation of the reference die or for a nearby set of process parameters) at that time t.

(2) Friction sensitivity assumption: If the frictional conditions at a particular point in contact for a reference deformation problem are those of sticking (sliding, respectively), the frictional conditions of this point at the same time for a nearby deformation problem will be that of sticking (sliding, respectively). Thus transition from a stick to a slip condition does not occur at a material point as a result of infinitesimal changes in the die shape or other process parameters.

Recall that in the direct contact problem, in addition to contact tractions, the regions of contact and the regions of slip/stick within the contact boundary are calculated. However, in the sensitivity analysis with the regularization assumptions introduced above, one needs to calculate only the sensitivities of the traction components, with the contact boundary and regions of stick/slip identified by the direct analysis.

Let us first introduce a proper notation for the sensitivity of a function $f = f(\mathbf{x})$. In the particular case of a die design problem, it is assumed that a variation in the die surface would not only result in a variation of the position $\mathbf{x}$, but also may result in a variation of the function f itself. The sensitivity of the function f denoted by $\overset{*}{[f(\mathbf{x})]}$ generally consists of two parts, the first part, $\overset{*}{f}$, denotes the contribution due to changes in the function f with $\mathbf{x}$ constant and the second part, $\nabla f \overset{*}{\mathbf{x}}$, denotes the contribution due to changes in the variable $\mathbf{x}$ with f constant, i.e.

$$\overset{*}{[f(\mathbf{x})]} = \overset{*}{f} + \nabla f \overset{*}{\mathbf{x}} \tag{69}$$

A calculation of the sensitivity $\overset{*}{\boldsymbol{\lambda}}$ of the contact traction is now developed. Figure 3 shows the schematic used to define the contact traction sensitivities. The analysis presented here is for die design problems and the change in the die shape is represented by $\overset{*}{\mathbf{y}}$.

In the present work, the sensitivity traction field $\overset{*}{\boldsymbol{\lambda}}$ is defined by differentiating with respect to the die surface the continuum contact constraints and then implementing these sensitivity contact constraints consistently with the analysis used in the direct contact problem. The variables $(\overset{*}{\boldsymbol{\lambda}}_n, \overset{*}{\bar{\xi}}_n)$ are assumed to be known as calculated from the time integration of the contact sensitivity problem from the previous time-step (time t_n). The corresponding unknown variables at time t_{n+1} are denoted as $(\overset{*}{\boldsymbol{\lambda}}, \overset{*}{\bar{\xi}})$, where for simplicity of notation, the subscript $(n+1)$ is omitted from variables that refer to time t_{n+1}. The solution of the direct deformation contact problem gives the contact tractions $\boldsymbol{\lambda}$ at time t_{n+1} and identifies regions of sticking and sliding.

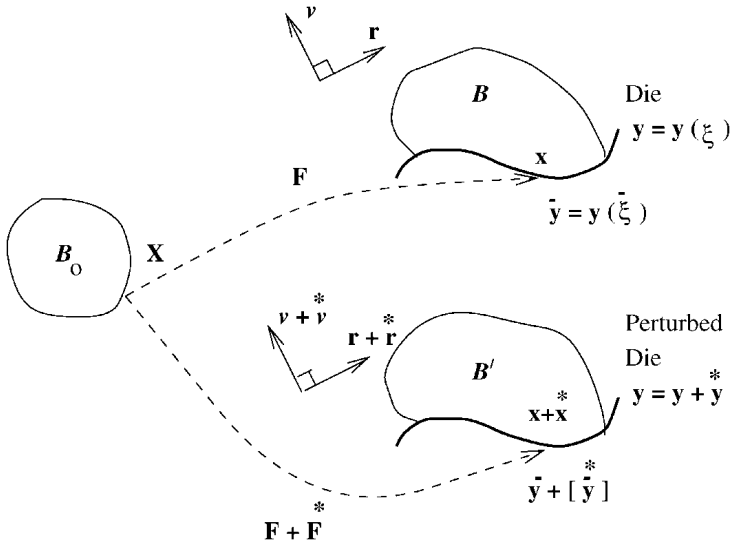

Figure 3. A schematic of the contact sensitivity problem for infinitesimal changes in the die shape.

Consideration of the strong form of the normal contact constraints in the direct deformation problem yields for points in contact $g(\mathbf{x}_{n+1}) = 0$ and $\lambda_N > 0$. Thus, the strong form of the normal contact sensitivity constraint is obtained as

$$\overset{*}{g(\mathbf{x}_{n+1})} = 0 \quad \text{and} \quad \overset{*}{\lambda}_N \in \Re$$

This is a direct result of the contact sensitivity assumption introduced earlier. The sensitivity $\overset{*}{\lambda}_N$ is treated as the Lagrange multiplier that enforces the continuum form of the normal contact sensitivity constraint. The following penalty form is used to enforce this constraint:

$$\overset{*}{\lambda}_N = \overset{*}{\lambda}_{N_n} + \varepsilon_N \overset{*}{g(\mathbf{x}_{n+1})} \tag{70}$$

where $\overset{*}{\lambda}_{N_n}$ is the sensitivity of the normal traction component at the beginning of the time integration step. The penalty parameter ε_N introduced above is generally not the same as the corresponding parameter used in the direct contact sub-problem (see Remark 3).

Consideration of the tangential contact constraints yields that for points in sticking contact, $\dot{\xi} = 0$. The corresponding sensitivity constraint (based on the friction sensitivity assumption) takes the form

$$\overset{*}{\dot{\xi}} = \dot{\overset{*}{\xi}} = 0$$

As in the case of the normal to the die sensitivity constraints, $\overset{*}{\lambda}_T$ is treated as the Lagrange multiplier that enforces the tangential to the die sensitivity constraints for the case of sticking contact. The following penalty formulation of the sticking sensitivity constraint is introduced:

$$\dot{\overset{*}{\xi}} = \frac{1}{\varepsilon_T} \overset{*}{\lambda}_T \tag{71}$$

Integration of this equation results in the following:

$$\overset{*}{\lambda}_{\mathrm{T}} = \overset{*}{\lambda}_{\mathrm{T}_n} + \varepsilon_{\mathrm{T}}(\overset{*}{\bar{\xi}} - \overset{*}{\bar{\xi}}_n) \tag{72}$$

where $\overset{*}{\lambda}_{\mathrm{T}_n}$ is the sensitivity of the tangential traction component at the beginning of the time integration step. The parameter ε_{T} can be selected independently of the corresponding parameter in the direct contact sub-problem.

Remark 3. Equations (70) and (72) are derived in a continuum contact sensitivity setting. An alternate formulation can be considered where the design differentiation of the corresponding discrete equations used in the augmented Lagrangian analysis in the direct contact sub-problem is carried out (i.e. of $\lambda_{\mathrm{N}} = \langle \lambda_{\mathrm{N}} + \varepsilon_{\mathrm{N}} g(\mathbf{x}_{n+1}^{(k)}) \rangle$ and $\lambda_{\mathrm{T}}^{\mathrm{trial}} = \lambda_{\mathrm{T}_n} + \varepsilon_{\mathrm{T}}(\bar{\xi}_{n+1}^{(k)} - \bar{\xi}_n) + \Delta\lambda_{\mathrm{T}}^{(k)}$, respectively). However, this interpretation requires that the penalty parameters ε_{N} and ε_{T} are identical in both the direct and sensitivity contact sub-problems. Such a restriction is unnecessary as it implies that the magnitude of the penalty parameters ε_{N} and ε_{T} in the sensitivity contact analysis is limited by corresponding values used in the direct contact problem. Indeed, recall that an augmented Lagrangian formulation instead of a penalty formulation is used in the direct contact algorithm because using large penalties to enforce contact and frictional constraints leads to ill-conditioning and convergence problems of the Newton algorithm that solves the non-linear direct deformation boundary value problem.

Remark 4. Solution of the direct deformation problem with moderate penalties within a time increment usually requires augmentations to accurately enforce the contact/frictional constraints. Derivation of the contact sensitivity sub-problem by differentiation with respect to the die of the discrete direct contact sub-problem (see Remark 3) will thus lead to a contact sensitivity algorithm that requires a number of iterations (augmentations). The sensitivity deformation problem is however a linear problem and augmentations are preferably avoided with a linear continuum sensitivity analysis.

As a result of the contact and frictional sensitivity assumptions, Equations (70) and (72) can be used here with high penalty parameters and no augmentations are necessary in the contact sensitivity analysis. For simplicity of notation, the contact sensitivity penalty parameters are denoted by ε_{N} and ε_{T}, even though they are not the same as the corresponding penalty parameters in the direct contact analysis.

In the case of slip, $\overset{*}{\lambda}_{\mathrm{T}}$ is well defined by the Coulomb friction law as follows:

$$\overset{*}{\lambda}_{\mathrm{T}} = \overset{*}{\left(\mu\lambda_{\mathrm{N}} \frac{1}{\|\boldsymbol{\tau}_1\|}\right)} \tag{73}$$

To simplify the above equation, the following relation is used:

$$\overset{*}{[\boldsymbol{\tau}_1(\bar{\mathbf{y}})]} = \overset{*}{[\bar{\mathbf{y}}_{,\xi}]} = \overset{*}{\bar{\mathbf{y}}}_{,\xi} + \bar{\mathbf{y}}_{,\xi\xi}\overset{*}{\bar{\xi}} \tag{74}$$

where $\overset{*}{\bar{\mathbf{y}}}_{,\xi}$ represents the contribution to the sensitivity due to changes in the shape $\mathbf{y}$ of the die.

Using the above equation, Equation (73) (applicable to a slip condition) simplifies as follows:

$$\overset{*}{\lambda}_{\mathrm{T}} = \frac{\overset{*}{\lambda}_{\mathrm{N}}}{\lambda_{\mathrm{N}}}\lambda_{\mathrm{T}} - \lambda_{\mathrm{T}}\left(\frac{\bar{\mathbf{y}}_{,\xi}\cdot\overset{*}{\bar{\mathbf{y}}}_{,\xi}}{\bar{\mathbf{y}}_{,\xi}\cdot\bar{\mathbf{y}}_{,\xi}}\right) - \lambda_{\mathrm{T}}\left(\frac{\bar{\mathbf{y}}_{,\xi}\cdot\bar{\mathbf{y}}_{,\xi\xi}}{\bar{\mathbf{y}}_{,\xi}\cdot\bar{\mathbf{y}}_{,\xi}}\right)\overset{*}{\xi} \tag{75}$$

One can thus complete the contact sensitivity description by writing the following equation for $\overset{*}{\boldsymbol{\lambda}}$:

$$\overset{*}{\boldsymbol{\lambda}} = \overset{*}{\boldsymbol{\lambda}}_{\mathrm{N}} - \overset{*}{\boldsymbol{\lambda}}_{\mathrm{T}}, \quad \overset{*}{\boldsymbol{\lambda}}_{\mathrm{N}} = \overset{*}{\lambda_{\mathrm{N}}\boldsymbol{\nu}(\bar{\mathbf{y}})}, \quad \overset{*}{\boldsymbol{\lambda}}_{\mathrm{T}} = \overset{*}{\lambda_{\mathrm{T}}\boldsymbol{\tau}_1(\bar{\mathbf{y}})} \tag{76}$$

where $\overset{*}{\boldsymbol{\lambda}}_{\mathrm{N}}$ and $\overset{*}{\boldsymbol{\lambda}}_{\mathrm{T}}$ are the sensitivities of the normal and tangential contact traction vectors, respectively. Using Equations (70), (74), (76b) and $\boldsymbol{\nu}(\bar{\mathbf{y}}) = \boldsymbol{\tau}_1(\bar{\mathbf{y}}) \times \mathbf{e}_2/\|\boldsymbol{\tau}_1(\bar{\mathbf{y}})\|$, the sensitivity of the normal contact traction vector can finally be expressed as follows:

$$\overset{*}{\boldsymbol{\lambda}}_{\mathrm{N}} = \overset{*}{g}\boldsymbol{\zeta}_1 + \overset{*}{\xi}\boldsymbol{\zeta}_2 + \boldsymbol{\zeta}_3 \tag{77}$$

where the vectors $\boldsymbol{\zeta}_i$ are defined by

$$\begin{aligned}
\boldsymbol{\zeta}_1 &= \varepsilon_{\mathrm{N}}\frac{(\bar{\mathbf{y}}_{,\xi}\times\mathbf{e}_2)}{\|\bar{\mathbf{y}}_{,\xi}\|}\\
\boldsymbol{\zeta}_2 &= \frac{\lambda_{\mathrm{N}}}{\|\bar{\mathbf{y}}_{,\xi}\|}\left[(\bar{\mathbf{y}}_{,\xi\xi}\times\mathbf{e}_2) - \left(\frac{\bar{\mathbf{y}}_{,\xi}\cdot\bar{\mathbf{y}}_{,\xi\xi}}{\bar{\mathbf{y}}_{,\xi}\cdot\bar{\mathbf{y}}_{,\xi}}\right)(\bar{\mathbf{y}}_{,\xi}\times\mathbf{e}_2)\right]\\
\boldsymbol{\zeta}_3 &= \overset{*}{\lambda}_{\mathrm{N}_n}\frac{(\bar{\mathbf{y}}_{,\xi}\times\mathbf{e}_2)}{\|\bar{\mathbf{y}}_{,\xi}\|} + \frac{\lambda_{\mathrm{N}}}{\|\bar{\mathbf{y}}_{,\xi}\|}\left[(\overset{*}{\bar{\mathbf{y}}}_{,\xi}\times\mathbf{e}_2) - \left(\frac{\bar{\mathbf{y}}_{,\xi}\cdot\overset{*}{\bar{\mathbf{y}}}_{,\xi}}{\bar{\mathbf{y}}_{,\xi}\cdot\bar{\mathbf{y}}_{,\xi}}\right)(\bar{\mathbf{y}}_{,\xi}\times\mathbf{e}_2)\right]
\end{aligned} \tag{78}$$

Similarly, using Equations (72) (for sticking friction) or (75) (for sliding friction), (74) and (76c), the sensitivity of the tangential contact traction vector $\overset{*}{\boldsymbol{\lambda}}_{\mathrm{T}}$ can be expressed as follows:

$$\overset{*}{\boldsymbol{\lambda}}_{\mathrm{T}} = \overset{*}{g}\,\boldsymbol{\vartheta}_1 + \overset{*}{\xi}\,\boldsymbol{\vartheta}_2 + \boldsymbol{\vartheta}_3 \tag{79}$$

If the material point is in sliding contact, then the vectors $\boldsymbol{\vartheta}_i$ take the form:

$$\begin{aligned}
\boldsymbol{\vartheta}_1 &= \frac{\varepsilon_{\mathrm{N}}}{\lambda_{\mathrm{N}}}\boldsymbol{\lambda}_{\mathrm{T}}\\
\boldsymbol{\vartheta}_2 &= \lambda_{\mathrm{T}}\bar{\mathbf{y}}_{,\xi\xi} - \left(\frac{\bar{\mathbf{y}}_{,\xi}\cdot\bar{\mathbf{y}}_{,\xi\xi}}{\bar{\mathbf{y}}_{,\xi}\cdot\bar{\mathbf{y}}_{,\xi}}\right)\boldsymbol{\lambda}_{\mathrm{T}}\\
\boldsymbol{\vartheta}_3 &= \frac{\overset{*}{\lambda}_{\mathrm{N}_n}}{\lambda_{\mathrm{N}}}\boldsymbol{\lambda}_{\mathrm{T}} - \left(\frac{\bar{\mathbf{y}}_{,\xi}\cdot\overset{*}{\bar{\mathbf{y}}}_{,\xi}}{\bar{\mathbf{y}}_{,\xi}\cdot\bar{\mathbf{y}}_{,\xi}}\right)\boldsymbol{\lambda}_{\mathrm{T}} + \lambda_{\mathrm{T}}\,\overset{*}{\bar{\mathbf{y}}}_{,\xi}
\end{aligned} \tag{80}$$

On the other hand, if the friction conditions are that of stick, ϑ_i take the form

$$\begin{aligned}\vartheta_1 &= \mathbf{0}\\ \vartheta_2 &= \varepsilon_T\,\bar{\mathbf{y}}_{,\xi} + \lambda_T\,\bar{\mathbf{y}}_{,\xi\xi}\\ \vartheta_3 &= \overset{*}{\lambda}_{T_n}\,\bar{\mathbf{y}}_{,\xi} - \varepsilon_T\,\overset{*}{\bar{\xi}}_n\,\bar{\mathbf{y}}_{,\xi} + \lambda_T\,\overset{*}{\bar{\mathbf{y}}}_{,\xi}\end{aligned} \tag{81}$$

If the contact conditions are frictionless, then $\vartheta_i = \mathbf{0}$.

Substitution of Equations (77) and (79) in Equation (76a) yields a concise expression for the sensitivity of the contact tractions as

$$\overset{*}{\boldsymbol{\lambda}} = \overset{*}{g}\,\boldsymbol{\gamma}_1 + \overset{*}{\bar{\xi}}\,\boldsymbol{\gamma}_2 + \boldsymbol{\gamma}_3 \tag{82}$$

where $\boldsymbol{\gamma}_i \equiv \boldsymbol{\zeta}_i - \vartheta_i$. The sensitivity $\overset{*}{\bar{\xi}}$ of the amount of inelastic slip is related to $\overset{*}{\mathbf{x}}$ (see Figure 3). The linear relationship between $\overset{*}{\bar{\xi}}$ and $\overset{*}{\mathbf{x}}$ is now developed. Consider the sensitivity of the relation $(\bar{\mathbf{y}} - \mathbf{x}) \cdot \boldsymbol{\tau}_1(\bar{\mathbf{y}}) = 0$ which expresses the fact that the closest point $\bar{\mathbf{y}}$ on the die to a point $\mathbf{x}$ is the projection of the point $\mathbf{x}$ on to the die. The sensitivity of the above relation is given by

$$(\mathbf{y}(\bar{\xi}) - \mathbf{x}) \cdot \overset{*}{\overline{[\mathbf{y}_{,\xi}(\bar{\xi})]}} + (\overset{*}{\overline{[\mathbf{y}(\bar{\xi})]}} - \overset{*}{\mathbf{x}}) \cdot \mathbf{y}_{,\xi}(\bar{\xi}) = 0 \tag{83}$$

The above expression can be simplified as follows:

$$\overset{*}{\bar{\xi}} = \mathbf{a} \cdot \overset{*}{\mathbf{x}} + b \tag{84}$$

where

$$\begin{aligned}\mathbf{a} &= \frac{\boldsymbol{\tau}_1(\bar{\mathbf{y}})}{\|\boldsymbol{\tau}_1(\bar{\mathbf{y}})\|^2[1 + g\kappa(\bar{\mathbf{y}})]}\\ b &= \frac{-[g\mathbf{v}(\bar{\mathbf{y}}) \cdot \overset{*}{\bar{\mathbf{y}}}_{,\xi} + \boldsymbol{\tau}_1(\bar{\mathbf{y}}) \cdot \overset{*}{\bar{\mathbf{y}}}]}{\|\boldsymbol{\tau}_1(\bar{\mathbf{y}})\|^2[1 + g\kappa(\bar{\mathbf{y}})]}\end{aligned} \tag{85}$$

where $\kappa(\bar{\mathbf{y}}) = \mathbf{v}(\bar{\mathbf{y}}) \cdot \mathbf{y}_{,\xi\xi}(\bar{\xi})/\|\boldsymbol{\tau}_1(\bar{\mathbf{y}})\|^2$ represents the curvature of the die at $\bar{\mathbf{y}}$.

The linear relationship between the sensitivity of the gap function $\overset{*}{\overline{g(\mathbf{x})}}$ and $\overset{*}{\mathbf{x}}$ can be obtained by the design differentiation of Equation (19) as follows:

$$\overset{*}{g} = \mathbf{v}(\bar{\mathbf{y}}) \cdot (\overset{*}{\bar{\mathbf{y}}} - \overset{*}{\mathbf{x}}) \tag{86}$$

Substitution of Equations (84) and (85) in Equation (82) results in the final expression for the sensitivity of the contact traction:

$$\overset{*}{\boldsymbol{\lambda}} = [(\boldsymbol{\gamma}_2 \otimes \mathbf{a}) - (\boldsymbol{\gamma}_1 \otimes \mathbf{v}(\bar{\mathbf{y}}))]\,\overset{*}{\mathbf{x}} + [(\mathbf{v}(\bar{\mathbf{y}}) \cdot \overset{*}{\bar{\mathbf{y}}})\boldsymbol{\gamma}_1 + b\boldsymbol{\gamma}_2 + \boldsymbol{\gamma}_3] \tag{87}$$

From Equations (63) and (87), one can conclude that the sensitivity of the contact tractions contributes to the force vector as well as the stiffness matrix in the weak form of the kinematic sensitivity problem (see the first term on the right-hand side of Equation (63)).

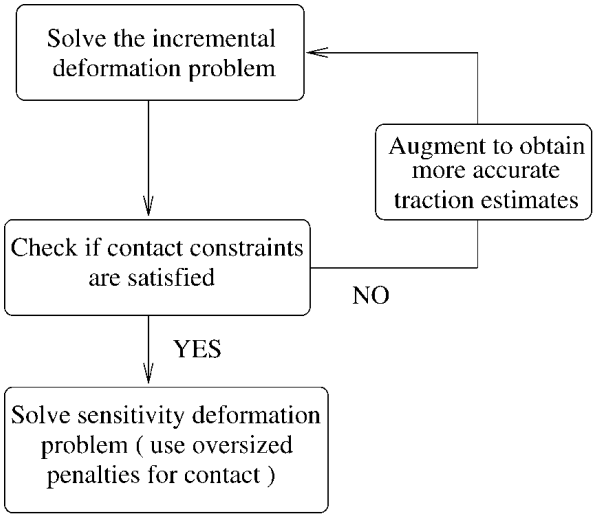

Figure 4. Solution procedure used in the contact sensitivity sub-problem. The penalty parameters ε_N and ε_T used in this analysis are much larger than those used in the direct contact sub-problem in which augmentations are usually necessary.

The initial conditions for the contact sensitivity algorithm at the beginning of the deformation at time t_0 are $(\overset{*}{\boldsymbol{\lambda}}_0, \overset{*}{\bar{\xi}}_0)$ which are given as follows:

$$\overset{*}{\boldsymbol{\lambda}}_0 = \mathbf{0}, \quad \overset{*}{\bar{\xi}}_0 = 0 \tag{88}$$

A summary of the time integration of the contact sensitivity sub-problem follows (Figure 4): Solve for the sensitivity of the deformation $\overset{*}{\mathbf{x}}$ at time t_{n+1}

$$\tilde{S}(\overset{*}{\mathbf{x}}, \tilde{\mathbf{u}}) = S(\overset{*}{\mathbf{x}}, \tilde{\mathbf{u}}) + S_c(\overset{*}{\mathbf{x}}, \tilde{\mathbf{u}}) = 0$$

Note: The above equation represents the linear sensitivity weak form, the solution of which requires input from the kinematic, constitutive and contact sensitivity sub-problems. The solution of this linear equation yields the sensitivity of the body configuration $\overset{*}{\mathbf{x}}$ corresponding to the body configuration $\mathbf{B}_{n+1}$.

The following values for the sensitivity of contact tractions are used in the solution for material points in contact (based on the computed body configuration $\mathbf{B}_{n+1}$ and the history of the sensitivity):

Sensitivity of normal traction:

Use $\overset{*}{\boldsymbol{\lambda}}_N$ from Equation (77)

Sensitivity of tangential traction:

IF $(\mathbf{x} \in \gamma_{stick})$ THEN

Use $\overset{*}{\boldsymbol{\lambda}}_T$ from Equations (79) and (81)

ELSE (sliding contact)

Use $\overset{*}{\boldsymbol{\lambda}}_T$ from Equations (79) and (80)

Remark 5. Implementation of the contact sensitivity algorithm obtained by differentiation of the discrete equations used in the direct contact sub-problem was also developed as part of this investigation. Such a contact sensitivity analysis uses the same penalty parameters ε_N and ε_T as the direct analysis and requires augmentations within a time increment. It has been determined that the method presented in this paper provides the same accuracy for the computed sensitivities of the contact tractions as this alternative method, although with a higher computational efficiency.

4. NUMERICAL RESULTS

A comprehensive set of numerical examples in the design of metal forming processes is considered here to validate the proposed computational framework and numerical algorithm. The CPU requirements of the present object oriented implementation are shown in a representative example. The computations were performed on an IBM RS-6000 workstation at the Cornell Theory Center. In all reported simulations three-noded cross triangular elements were used. Unless otherwise stated, the penalty parameters for the sensitivity contact problem are selected as $\varepsilon_N = 10^8$ and $\varepsilon_T = 10^4$. The workpiece material chosen in all examples is Al 1100-O at 673 K. The constitutive model for this material is taken from Brown *et al.* [27] and is summarized in Appendix B.

4.1. Accuracy investigations

4.1.1. Sensitivity calculations in axisymmetric extrusion (*Example 1*). An axisymmetric extrusion of a cylindrical workpiece is considered through a curved die. The initial radius of the workpiece is 1 cm and the initial height is 2 cm. A friction coefficient of 0.01 is assumed at the die–workpiece interface.

A degree six ($n=6$) Bézier curve is used to represent the die shape:

$$r = \sum_{i=1}^{n+1} C_i f_i(\alpha) \tag{89}$$

$$z = \alpha \ (\text{in cm}) \tag{90}$$

Here $\alpha \in [0,1]$, and $C_i,\ i=1,\ldots,(n+1)$, are algebraic control parameters (points). The Bernstein functions $f_i(\alpha),\ i=1,\ldots,(n+1)$, are defined as follows:

$$f_i(\alpha) = \frac{n!}{(i-1)!(n-i+1)!}\alpha^{i-1}(1-\alpha)^{n-i+1} \tag{91}$$

In order to obtain the same reduction for different die design parameters, the parameters C_1 and C_7 are selected such that $C_1 = 1.0$ cm and $C_7 = 0.866$ cm. Such a selection results in a fixed cross-sectional area reduction of 25 per cent. In addition, to allow the workpiece to enter and leave the die zone smoothly, the die curve at the entrance and exit is restricted to be perpendicular to the radial axis. This is accomplished by selecting $C_2 = C_1$ and $C_6 = C_7$.

With the above selection of the parameters C_i, there are three remaining die design parameters $(\beta_1, \beta_2, \beta_3) \equiv (C_3, C_4, C_5)$. The initial values are arbitrary, and the reference (initial) die is selected such that

$$\beta_1 = (3C_1 + C_7)/4, \quad \beta_2 = (C_1 + C_7)/2, \quad \beta_3 = (C_1 + 3C_7)/4$$

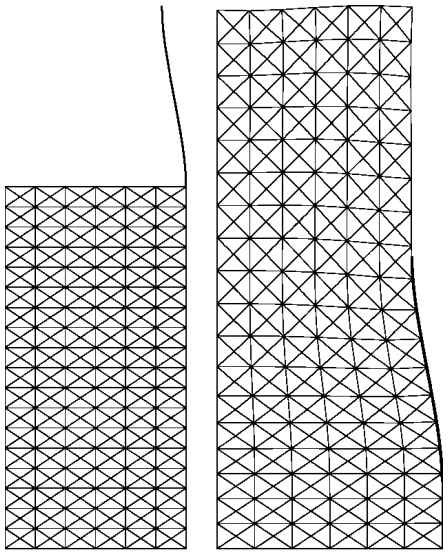

Figure 5. The initial and steady-state ($t = 170\,\mathrm{s}$) grids shown along with the initial guess of the die shape (Example 1).

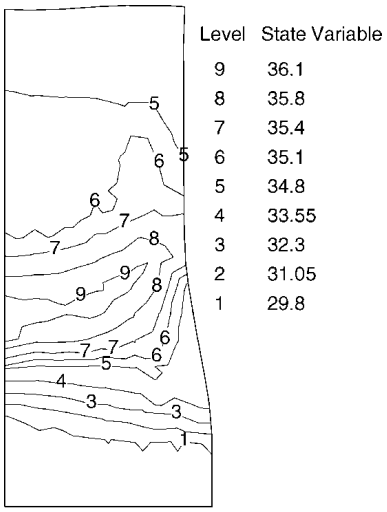

Figure 6. Steady-state distribution of the state variable s (in MPa) (Example 1).

Table I. Simulation parameters for the frictional extrusion of a 1100-Al billet (Example 1).

Parameter	Value
Energy error norm	1.0E − 07
Displacement L_2 error norm	1.0E − 07
Normal penalty for contact	1.0E + 06
Tolerance for gap	1.0E − 06
Tangent penalty for contact	1.0E + 03
Tolerance for friction condition	1.0E − 06

The initial die shape (length = 1 cm) is shown in Figure 5. A finite element mesh of 6×18 cross-triangular elements is considered (Figure 5). The extrusion velocity is 0.01 cm/s. A fixed time step of $\Delta t = 0.25\,\mathrm{s}$ is used. The parameters used in the simulation are given in Table I. The time at which the process reached steady-state conditions at the exit was computed as $t = 170\,\mathrm{s}$. The grid at this time is also shown in Figure 5.

Figure 6 shows the steady-state contour plot of the state variable s. In more detail, the state variable distribution s along the die exit is shown in Figure 7 demonstrating that steady-state conditions are achieved at $t = 170\,\mathrm{s}$. Figures 8–10 show the steady-state contours of the sensitivity $\overset{*}{s}$ with respect to the design parameters $(\beta_1, \beta_2, \beta_3)$ using the DDM (direct differentiation) and the FDM (finite difference) methods. The FDM results are obtained using the results of the direct analysis and a forward difference approximation for a perturbation of each of the design variables by 10^{-3} cm. Figure 11 shows a comparison of the sensitivity $\overset{*}{s}$ with respect to each of the design

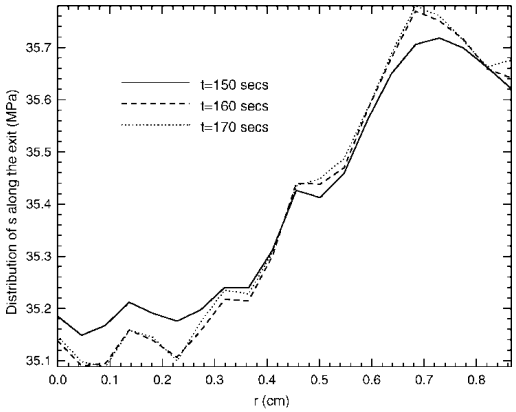

Figure 7. The distribution of the state variable s along the exit at various process times (Example 1).

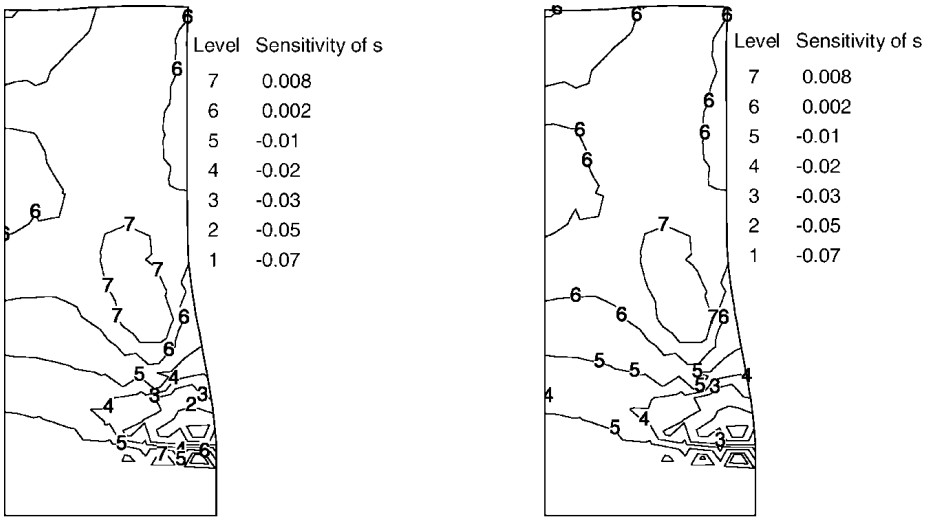

Figure 8. Contours of the steady-state sensitivity of the state variable s (in MPa) with respect to β_1 computed using the DDM and FDM methods (Example 1).

parameters along the die exit using the DDM and the FDM at steady state. The results match quite well.

4.1.2. Evaluation of the accuracy of the computed sensitivities of contact tractions in an open die forging process (*Example 2*). In this example, the accuracy of the computed sensitivities of contact tractions with respect to the speed of a flat die in an open die forging process is examined, i.e. the forging rate V is here taken as the process (design) parameter. Variations in the forging rate affect the dissipated energy during upsetting and so it is important to be able to model the sensitivity fields as a result of this variation.

The initial cylindrical workpiece of radius 1.00 mm and height 3.00 mm is discretized using 576 triangular finite elements. As a result of the symmetry of the problem, only a quarter of the

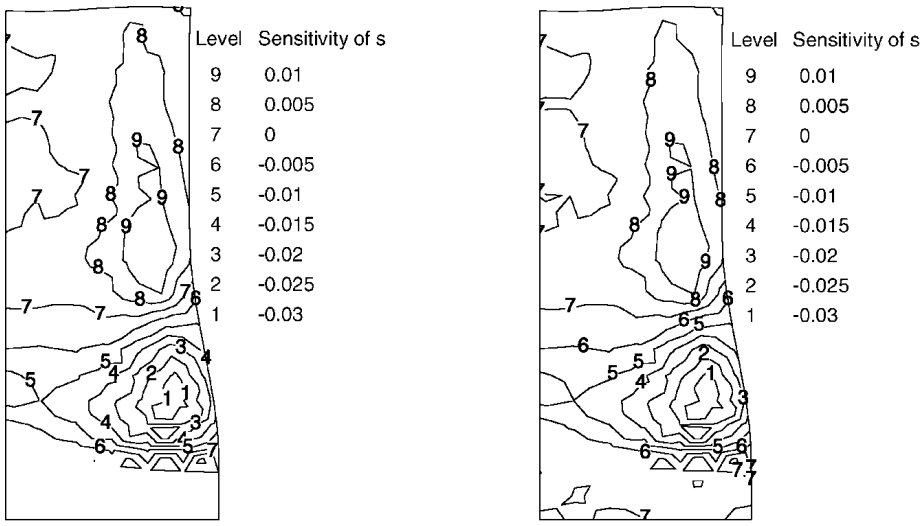

Figure 9. Contours of the steady-state sensitivity of the state variable s (in MPa) with respect to β_2 computed using the DDM and FDM methods (Example 1).

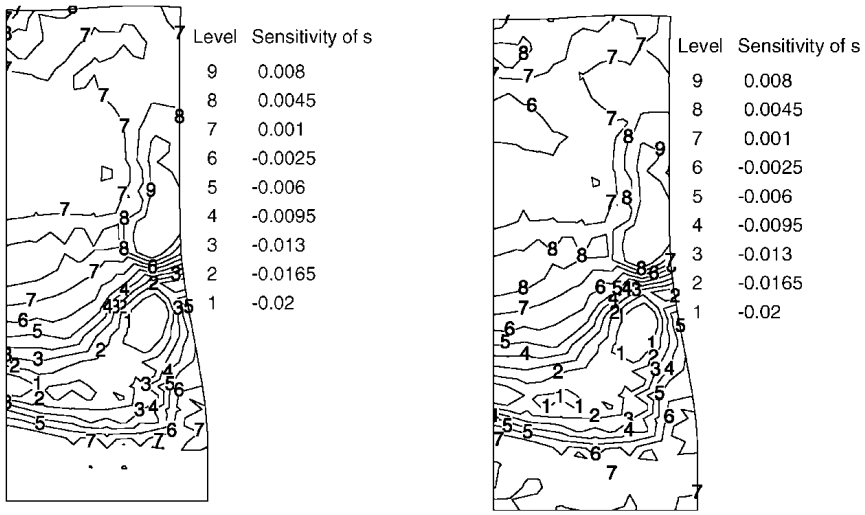

Figure 10. Contours of the steady-state sensitivity of the state variable s (in MPa) with respect to β_3 computed using the DDM and FDM methods (Example 1).

work-piece is modelled (Figure 12). The specified forging velocity for the reference problem is $V = 0.01$ mm/s and the workpiece is allowed to deform to 80 per cent of its initial height at which time the sensitivity fields are monitored. The various simulation parameters are given in Table II. The FDM values are computed corresponding to a variation of $\delta V = 10^{-4}$ mm/s.

The accuracy of the contact sensitivity algorithm introduced in this paper (see Figure 4) is investigated here with the penalty parameters in the sensitivity algorithm selected as $\varepsilon_N = 1.0E+08$ and $\varepsilon_T = 1.0E+06$. In addition, an alternative simulation is also performed with smaller contact

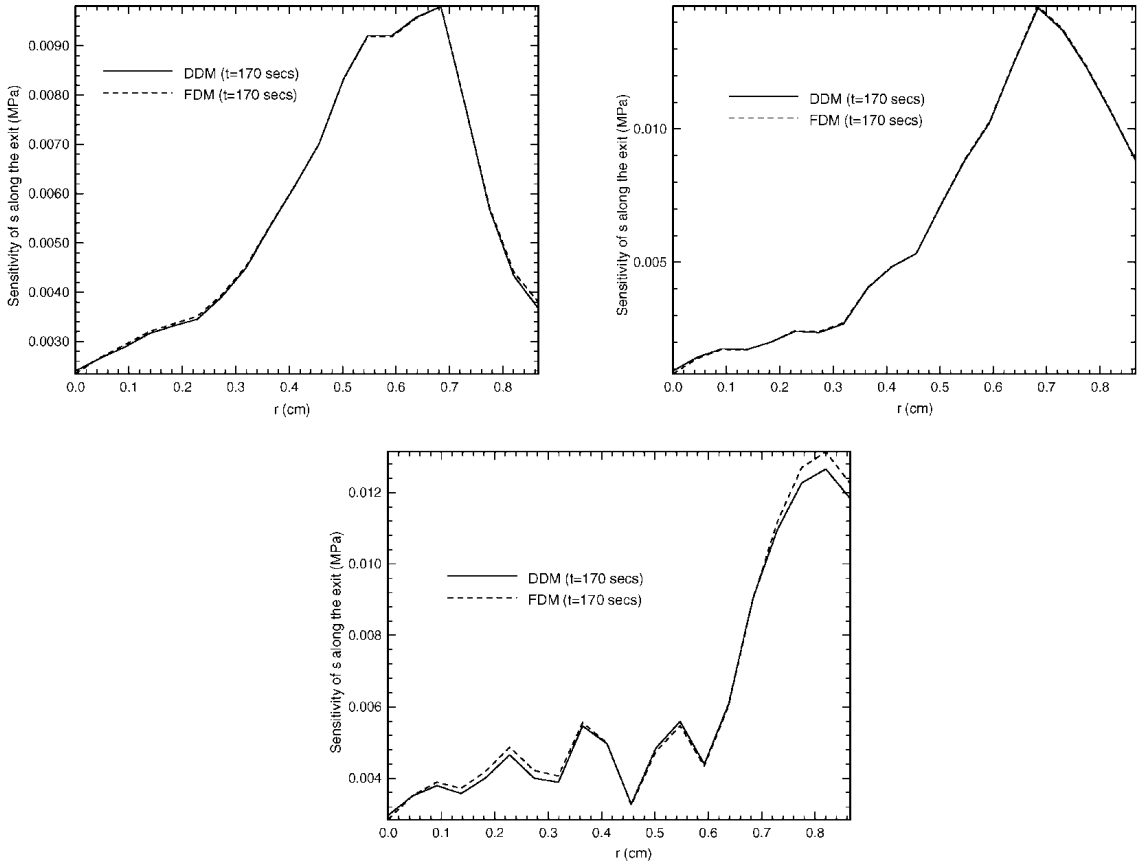

Figure 11. Comparison of steady-state values of $\overset{*}{s}$ at the exit corresponding to β_1, β_2 and β_3, respectively, computed using the DDM and FDM methods (Example 1).

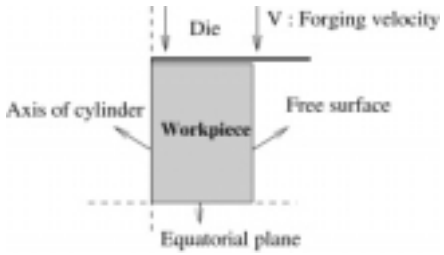

Figure 12. Axisymmetric upset forging for parameter sensitivity analysis with respect to the die speed (Example 2).

penalty parameters. As mentioned in Remarks 4 and 5, augmentations are required within a time step for such a choice. The penalty parameters for this simulation are selected to be the same as the corresponding parameters in the direct contact problem. Such an alternative simulation can be thought of as the regularized derivative of the corresponding discrete contact algorithm of the direct analysis.

Table II. Simulation parameters for the frictional open die forging of an axisymmetric 1100-Al billet (Example 2).

Parameter	Value
Energy error norm	1.0E − 08
Displacement L_2 error norm	1.0E − 08
Normal penalty for contact	1.0E + 07
Tangent penalty for contact	1.0E + 05
Tolerance for gap	1.0E − 08
Tolerance for friction	1.0E − 06

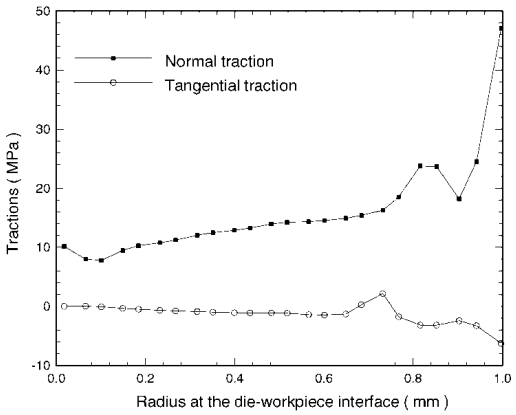

Figure 13. Distribution of the normal and tangential contact traction components at the final state for the axisymmetric frictional upsetting process with a reference die velocity of 0.01 mm/s (Example 2).

In order to validate the parameter sensitivity problem for processes involving frictional contact, a moderate friction coefficient of 0.4 is chosen to allow for variable regions of stick and slip at the contact interface. Figure 13 depicts the variation of the normal and tangential tractions at the die–workpiece interface using the reference die velocity. Figure 14 shows the variation of $\partial\lambda_N/\partial V$ and $\partial\lambda_T/\partial V$ along the radius in the deformed configuration at the die–workpiece contact interface. In general the FDM and DDM results (using the present contact sensitivity algorithm and the alternative contact sensitivity algorithm mentioned above) agree very well. It is observed that the DDM method is able to accurately predict the tangential traction derivatives in regions where there is a transition from stick to slip or vice versa. This is evident at the sharp peak at radius $r \approx 0.7$ in Figure 14 where there is a transition from sticking friction (inner radii) to sliding friction (outer radii). The non-smooth behaviour at this location is the result of the Coulomb law used to model friction. Small oscillations in the sensitivities (observed both in the FDM and DDM methods) are due to the instability in the finite element implementation of the direct deformation problem as a result of the reduced numerical quadrature used in the treatment of near-incompressibility and is currently being investigated.

The computational savings using the present DDM method are substantial for problems where the contact conditions are complex and is therefore the recommended method that is used in the remaining of this paper.

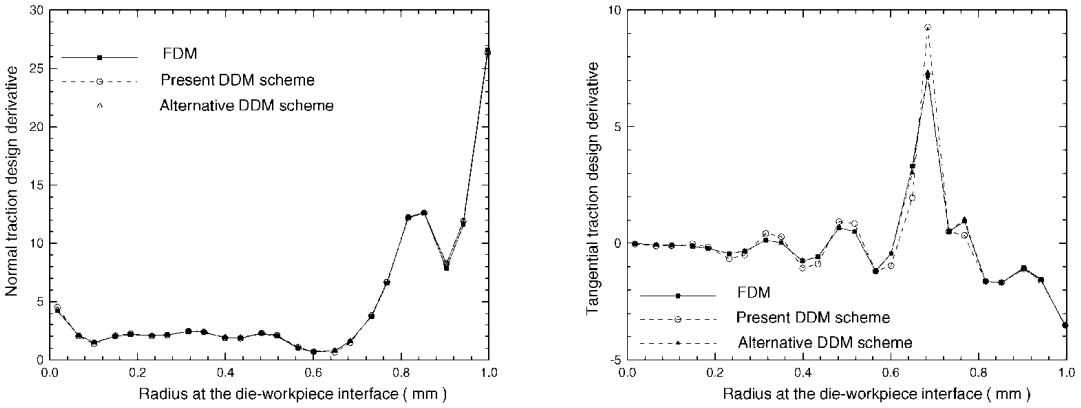

Figure 14. Comparison of the design derivatives $\partial\lambda_N/\partial V$ and $\partial\lambda_T/\partial V$ computed with the DDM and FDM methods for the axisymmetric frictional upsetting process (Example 2).

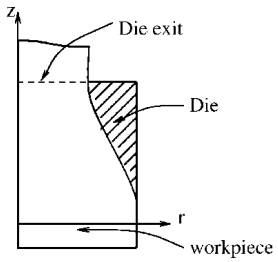

Figure 15. Die design for uniform distribution of the state variable s at the exit location in axisymmetric extrusion (Example 3).

4.2. Using sensitivity calculations for die design problems

4.2.1. Die design for uniform material state in an extruded product (*Example 3*). In this example, the die parameters in the Bézier representation given in Section 4.1.1 are designed such that the distribution of s at the die exit (see Figure 15) is as uniform as possible, i.e. one is interested in calculating the die parameters such that the following function is minimized:

$$f(\boldsymbol{\beta}_p) = \sum_{i=1}^{N} (s_i - \bar{s})^2 \tag{92}$$

where s_i $(i = 1, \ldots, N)$ are N $(= 20)$ discrete (equally spaced) state variable s values along the radius at the exit (in the particular example, along $z = 1.0\,\text{cm}$) and $\bar{s} = \sum_{i=1}^{N}(1/N)s_i$ is the mean value of the distribution of s along the exit.

The extrusion conditions are identical to those given in Example 1. The initial mesh is shown in Figure 5 with 6×18 cross triangular elements. A fixed time step $\Delta t = 0.25\,\text{s}$ is considered and the steady-state process time is taken as $t = 170\,\text{s}$.

The computed sensitivity fields are used to evaluate the gradient of the objective function. Various optimization methods have been tested for this design problem. Figure 16 shows the objective function values as well as the norm of the gradient of the objective function, during the iterations

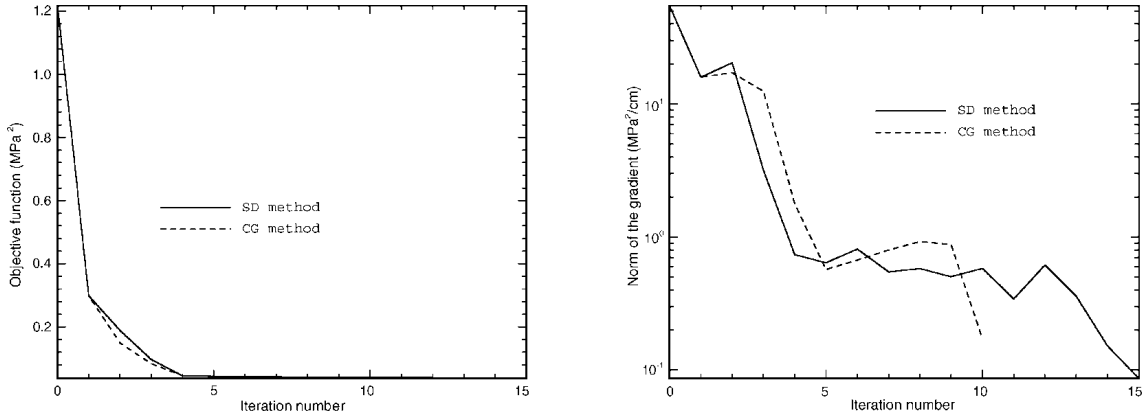

Figure 16. The objective function and the norm of gradient of the objective function, respectively, versus the iteration index (Example 3).

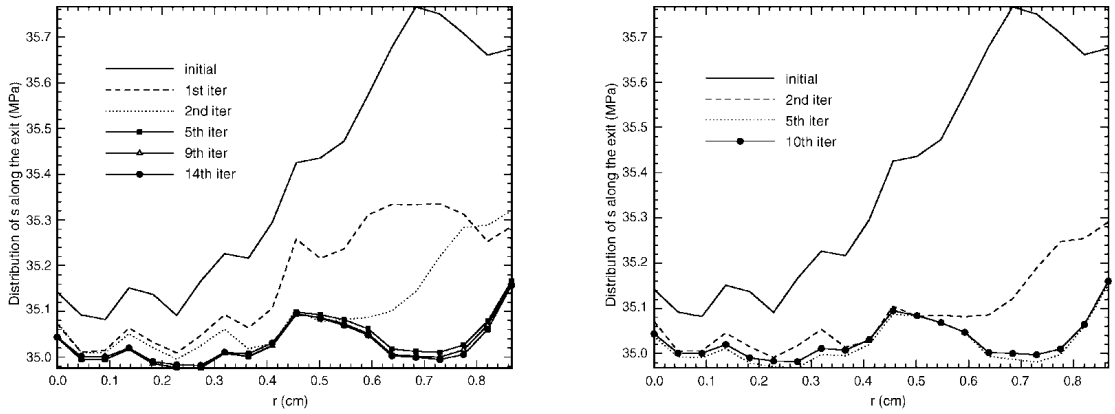

Figure 17. Distribution of s along the exit using the SD and CG methods, respectively (Example 3).

using the steepest descent (SD) and conjugate gradient (CG) methods. Figure 17 shows the distribution of s along the exit at the final time during various optimization iterations. Convergence is achieved after 14 iterations. The computed die shapes during the initial and following optimization iterations using the SD and CG methods are shown in Figure 18. Both optimization methods result in the same optimal die.

The computing statistics for the optimization of the die shape in one iteration are summarized in Table III. In the FDM method, one optimization iteration includes 4 direct problems. In the DDM method, one optimization iteration includes 1 direct problem and 3 sensitivity sub-problems The DDM method results in savings of about 64 per cent compared to the FDM method.

4.2.2. Die design for minimum required extrusion force for a given reduction ratio (*Example 4*). The same Bézier approximation and design parameters are used as in the earlier extrusion examples. The die design parameters are calculated such that the required extrusion force is minimized.

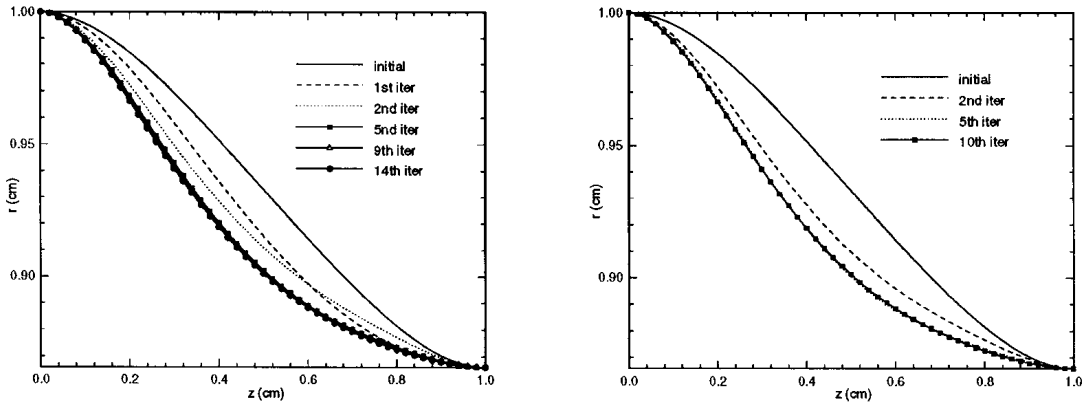

Figure 18. The computed die shapes during various iterations using the SD and CG methods, respectively (Example 3).

Table III. CPU time (in hours) for the extrusion die design problem (Example 3).

Direct problem	2.5
Sensitivity sub-problem	0.3
1 optimization iteration with FDM	10.0
1 optimization iteration with DDM	3.6

The required force is expressed as follows:

$$F_{\mathrm{e}} = \int_{\partial \mathbf{B}_n} \boldsymbol{\lambda} \cdot \mathbf{e}_Z \, \mathrm{d}A_n \tag{93}$$

and the sensitivity $\overset{*}{F}_{\mathrm{e}}$ can be expressed as

$$\overset{*}{F}_{\mathrm{e}} = \int_{\partial \mathbf{B}_n} \overset{*}{\boldsymbol{\lambda}} \cdot \mathbf{e}_Z \, \mathrm{d}A_n \tag{94}$$

where the integrations over the boundary $\partial \mathbf{B}_n$ are non-zero only on the boundary $\boldsymbol{\Gamma} \subset \partial \mathbf{B}_n$ where contact occurs.

The initial design parameters are selected as the optimal parameters evaluated in Example 3, i.e. $\beta_1 = 0.90829\,\mathrm{cm}$, $\beta_2 = 0.88793\,\mathrm{cm}$, and $\beta_3 = 0.88279\,\mathrm{cm}$. Due to the finite element implementation of the contact problem, the computed extrusion force for a given die is oscillatory (Figure 19). However, when the stroke is greater than 1.2 cm, the mean extrusion force remains constant. The average force between stroke 1.2 and 1.7 cm is used here as the objective function to be minimized. Figure 20 shows the sensitivity of the extrusion force versus stroke with respect to the three die design parameters, using both the FDM and the DDM methods. The results agree quite well. In the FDM calculations, the increments $\Delta\beta_i$, $i = 1, 2, 3$, were taken as $10^{-3}\,\mathrm{cm}$.

A quasi-Newton method with a BFGS update of the Hessian is used to minimize the steady-state extrusion force. The objective function is approximated at each optimization step as a quadratic function along the descent direction. Three different step sizes are selected along the descent

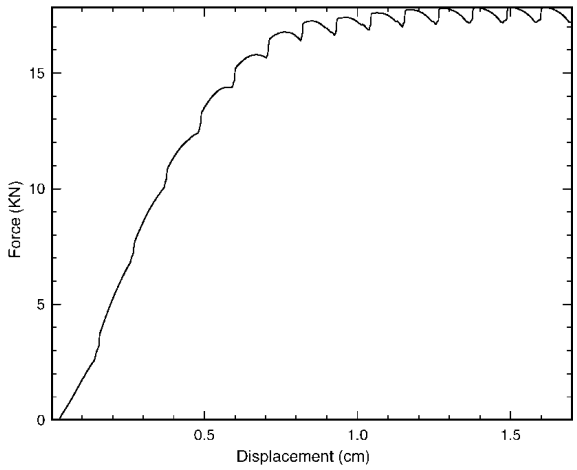

Figure 19. The extrusion force versus stroke for the initial die design (Example 4).

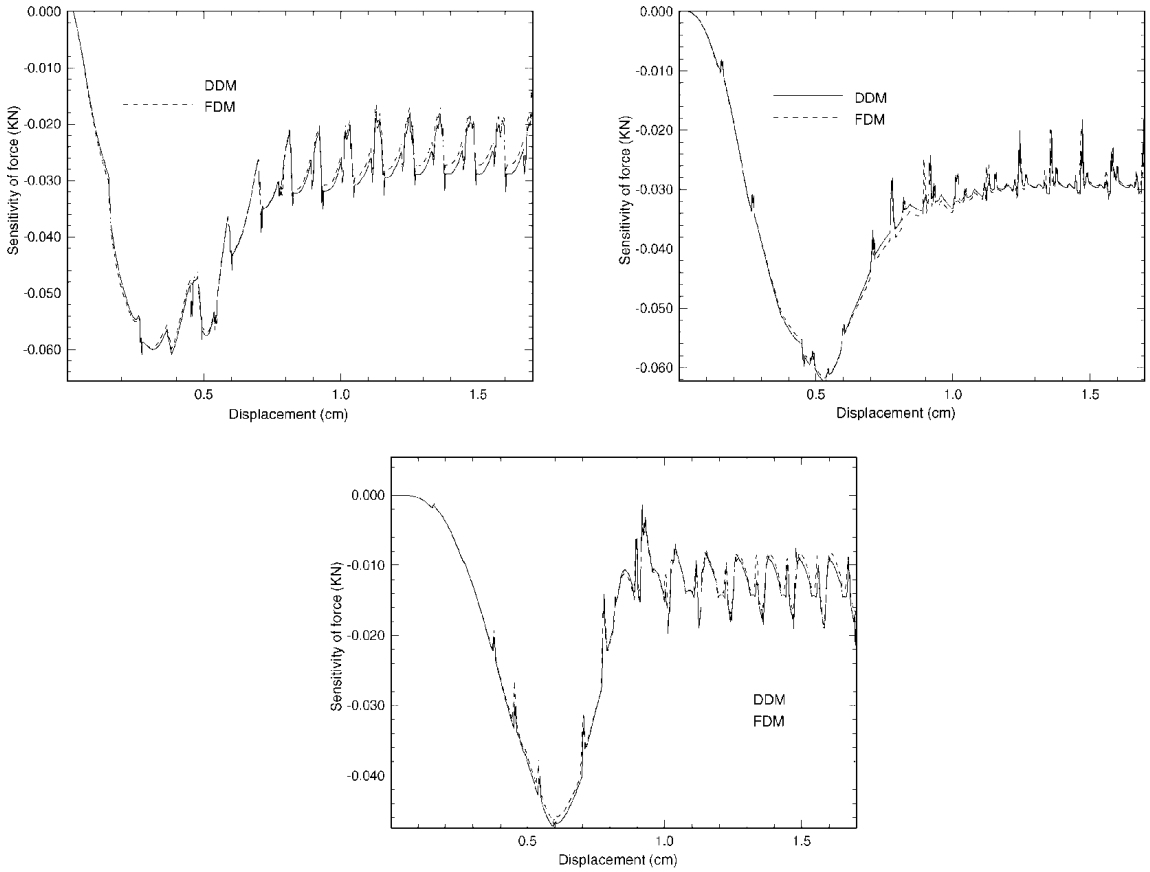

Figure 20. The sensitivity of the steady-state extrusion force with respect to β_1, β_2 and β_3, respectively (Example 4).

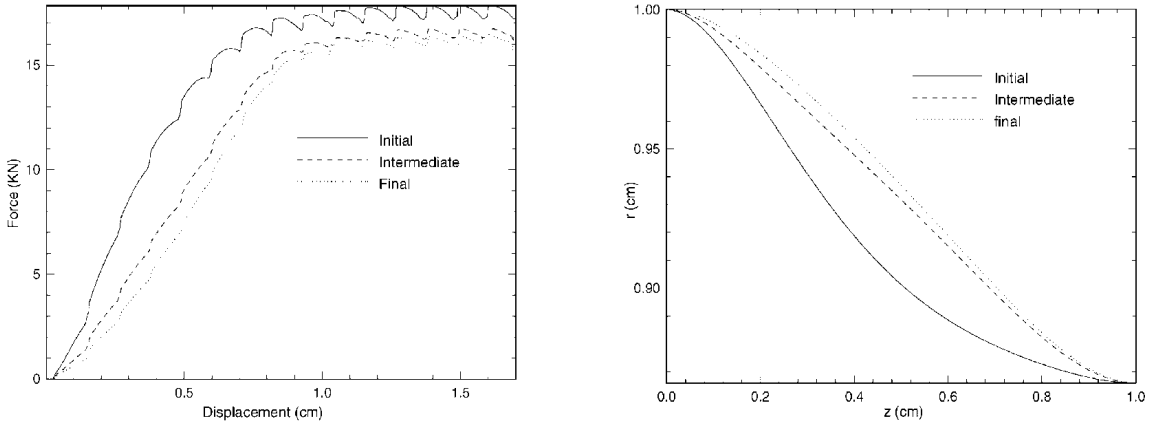

Figure 21. The extrusion force versus stroke and the various die shapes, respectively, computed during the optimization process (Example 4).

direction and the direct problem is simulated with the corresponding design variables to obtain the values of the objective function. The three computed values of the objective function define a local quadratic approximation that can be used to find the minimum in the descent direction. The extrusion force–stroke curve and the corresponding die shapes during the optimization processes are shown in Figure 21. The optimized die is quite flat in comparison to the initial die.

4.2.3. Die design in axisymmetric open-die forging to obtain a product of desired shape (*Example 5*). Consider an arbitrary curved die with which an axisymmetric cylindrical workpiece is forged for a given reduction resulting in a product of some final shape. In this example, we would like to use an optimization scheme with the present sensitivity analysis to recover the die shape starting from the shape of the free surface of the final product. One could start from the whole shape of the final product. However, since the top surface in principle defines the desired die, only the free surface is used in the present calculations. Such calculations will proceed in an iterative manner starting with a flat die until a die is found that results in the desired shape of the free surface in the final product. A single stage forging process cannot always produce a product of desired shape and generally a multi-stage process is needed. However, based on the direct analysis that produced the desired shape in the current application, it is known that a die does exist that results in a product of the desired free surface shape after open-die forging of the workpiece.

The initial radius of the workpiece is 1 cm and the initial height 3 cm. A friction coefficient of 1.0 is assumed along the die–workpiece interface. A degree four ($n=4$) Bézier curve is used to represent the die shape:

$$r = 1.5\alpha \text{ (in cm)}, \quad z = \sum_{i=1}^{n+1} C_i f_i(\alpha)$$

Here $\alpha \in [0,1]$, and C_i, $i=1,\ldots,(n+1)$, are algebraic parameters with $f_i(\alpha)$, $i=1,\ldots,(n+1)$, the Bernstein basis functions (see Equation (91)). To account for the axisymmetry of the problem, the parameters C_1 and C_2 are selected as follows $C_1 = C_2$ $(=1.8\,\text{cm})$. A particular die is defined with $(\beta_1,\beta_2,\beta_3) \equiv (C_3,C_4,C_5)$ with initial values of $(2.04, 2.13, 2.05)$ cm. This die shape, the initial workpiece and the final product resulting after 33.33 per cent height reduction (at $r=0$) are shown

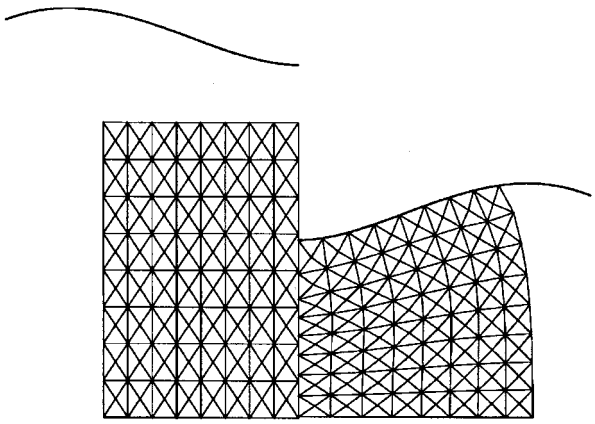

Figure 22. The initial workpiece and selected die. After 33.33 per cent height reduction (at $r = 0$), the product shown in the right of the figure results. The shape of the free surface of this product is used as the desired shape in the optimization analysis (Example 5).

Table IV. Simulation parameters for the design of an open die forging process (Example 5).

Parameter	Value
Energy error norm	1.0E − 07
Displacement L_∞ error norm	1.0E − 07
Normal penalty for contact	1.0E + 05
Tangent penalty for contact	1.0E + 04
Tolerance for gap	1.0E − 05
Tolerance for friction condition	1.0E − 05

in Figure 22. The die speed is taken as 0.01 cm/s. Due to axisymmetry, only 1/4 of the workpiece cross-section is modelled using a mesh of 8×8 cross-triangular finite elements. The time step was selected as $\Delta t = 0.2$ s. The remaining parameters used in this direct simulation are given in Table IV.

In the present design problem, one is given the initial shape of the workpiece (Figure 22(a)) and is interested in finding the die shape that after a 33.33 per cent height reduction (at $r = 0$) results in a free surface of the final product as that given in Figure 22(b). It is obvious that the solution to this problem corresponds to the curved die defined earlier. The CG method is used to calculate the descent direction during iterations and a line search method is used to calculate the step size in each optimization step. Figure 23 shows the final workpiece and the computed dies during the optimization process. Figure 24 shows the values of the objective function as well as the norm of the gradient of the objective function versus the number of iterations. It is apparent that after four iterations, the die shape has converged to the expected solution of this design problem.

Such a die design problem is essential in multi-stage process design in which various intermediate preforms have to be designed. Such applications will be reported in a forthcoming publication [34].

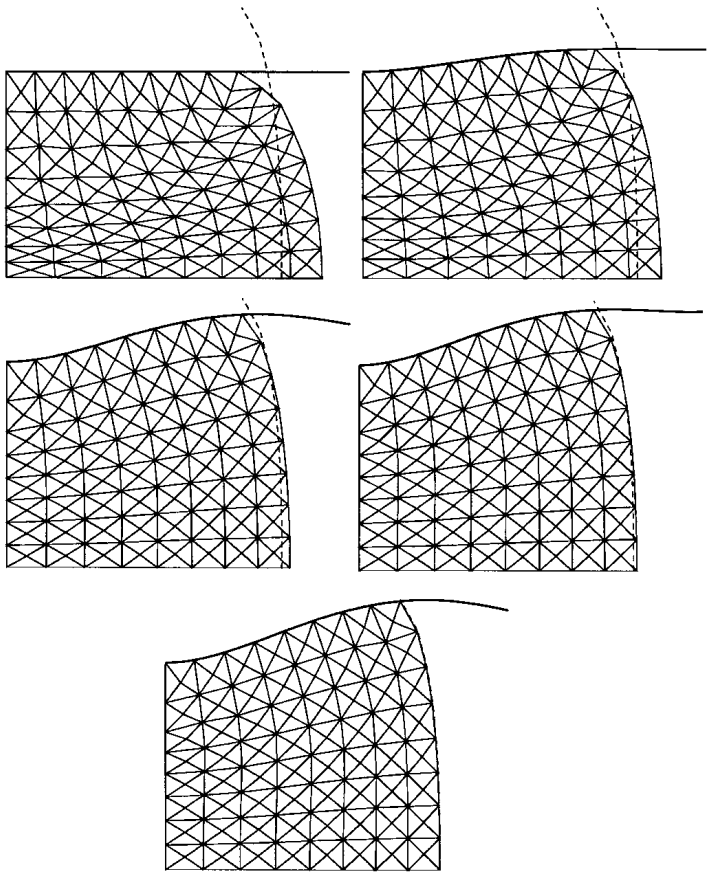

Figure 23. The final workpiece during various steps in the optimization process. The initial, 1st, 2nd, 3rd and final (4th) iterations are shown together with the desired shape of the free surface in the final product (Example 5).

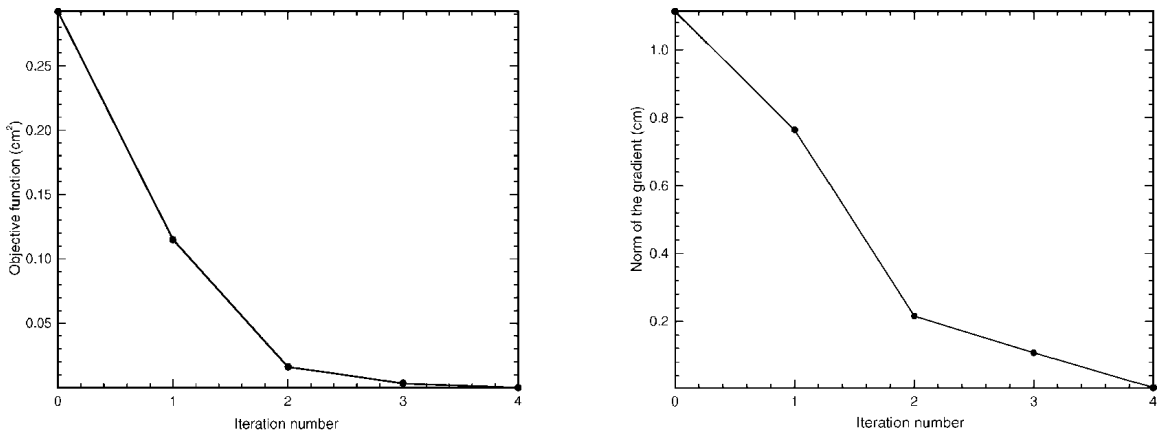

Figure 24. The objective function and the norm of the gradient of the objective function versus the number of iterations for the open-forging die design problem (Example 5).

5. CONCLUSIONS

An accurate and efficient continuum sensitivity analysis was presented for the design of metal forming processes. The developed methodology is applicable for the calculation of the sensitivities of the deformation, stresses and state variables with respect to variations in the die surface as well as variations in other (non-shape related) process parameters.

An effective method was presented for computing the sensitivities of the contact tractions. The method is developed by differentiation of the continuum contact and frictional constraints after a number of regularizing assumptions were introduced. The linearity of the sensitivity algorithm was preserved and no iterations or augmentations were required in the calculation of various sensitivity fields.

Various examples were presented to demonstrate the accuracy and potential of the developed sensitivity analysis. Both extrusion and open-die forging processes were considered. Preform design problems based on the present analysis are addressed in a companion paper [33].

APPENDIX A. DERIVATION OF THE LINEAR RELATION BETWEEN $\overset{*}{\mathbf{F}}{}^{\mathrm{e}}_{n+1}$ AND $\overset{*}{\mathbf{F}}_{n+1}$

A sequence of steps is followed in order to express $\overset{*}{\mathbf{F}}{}^{\mathrm{e}}_{n+1}$ as a linear function of $\overset{*}{\mathbf{F}}_{n+1}$. The variable $\mathbf{D}_{n+1}$ is introduced as follows:

$$\mathbf{D}_{n+1} \equiv [\mathbf{F}^{\mathrm{e}}]^{-1}_{n+1}(\overset{*}{\mathbf{F}}_{n+1}\ \mathbf{F}^{-1}_{n+1})\mathbf{F}^{\mathrm{e}}_{n+1} \tag{A1}$$

and $\mathbf{G}_{n+1}$ is defined as follows:

$$\mathbf{G}_{n+1} = \mathbf{D}_{n+1} - \mathbf{C}_{n+1} \tag{A2}$$

where $\mathbf{C}_{n+1}$ is given by Equation (36). For an isotropic hyperelastic model with shear modulus $\mathscr{G}$, one can write the following:

$$\overset{*}{\bar{\mathbf{T}}}{}'_{n+1} = 2\mathscr{G}\overset{*}{\bar{\mathbf{E}}}{}^{\mathrm{e}}_{n+1} - \frac{2\mathscr{G}}{3}\mathrm{tr}(\overset{*}{\bar{\mathbf{E}}}{}^{\mathrm{e}}_{n+1})\mathbf{I} \tag{A3}$$

As shown in Reference [26],

$$\mathrm{tr}(\overset{*}{\bar{\mathbf{E}}}{}^{\mathrm{e}}_{n+1}) = \mathrm{tr}(\overset{*}{\mathbf{U}}{}^{\mathrm{e}}_{n+1}[\mathbf{U}^{\mathrm{e}}]^{-1}_{n+1}) \tag{A4}$$

Using the tensor property $\mathrm{tr}(\mathbf{AB}) = \mathrm{tr}(\mathbf{BA})$ and the sensitivity of the the polar decomposition of $\mathbf{F}^{\mathrm{e}}_{n+1}$, one can show that

$$\mathrm{tr}(\overset{*}{\mathbf{F}}{}^{\mathrm{e}}_{n+1}[\mathbf{F}^{\mathrm{e}}]^{-1}_{n+1}) = \mathrm{tr}(\overset{*}{\mathbf{U}}{}^{\mathrm{e}}_{n+1}[\mathbf{U}^{\mathrm{e}}]^{-1}_{n+1}) \tag{A5}$$

and using Equation (A4) conclude that

$$\mathrm{tr}(\overset{*}{\mathbf{F}}{}^{\mathrm{e}}_{n+1}[\mathbf{F}^{\mathrm{e}}]^{-1}_{n+1}) = \mathrm{tr}(\overset{*}{\bar{\mathbf{E}}}{}^{\mathrm{e}}_{n+1}) \tag{A6}$$

Using Equations (41), (A2) and (A6) and the fact that deviatoric tensors are traceless, one arrives at the following equation:

$$\mathrm{tr}(\overset{*}{\bar{\mathbf{E}}}{}^{\mathrm{e}}_{n+1}) = \mathrm{tr}(\mathbf{G}_{n+1}) \tag{A7}$$

By considering the dot product of Equation (41) with $\bar{\mathbf{T}}'_{n+1}$, one can eliminate $\overset{*}{\tilde{\sigma}}_{n+1}$ from this equation. This is shown by the sequence of steps that follow.

Let us first consider the quantity, $([\mathbf{F}^{\mathrm{e}}]^{-1}_{n+1}\overset{*}{\mathbf{F}}{}^{\mathrm{e}}_{n+1}) \cdot \bar{\mathbf{T}}'_{n+1}$. Using the sensitivity of the polar decomposition of $\mathbf{F}^{\mathrm{e}}_{n+1}$, one can write,

$$\{[\mathbf{F}^{\mathrm{e}}]^{-1}_{n+1}\overset{*}{\mathbf{F}}{}^{\mathrm{e}}_{n+1}\} \cdot \bar{\mathbf{T}}'_{n+1} = \{[\mathbf{U}^{\mathrm{e}}]^{-1}_{n+1}([\mathbf{R}^{\mathrm{e}}]^{\mathrm{T}}_{n+1}\overset{*}{\mathbf{R}}{}^{\mathrm{e}}_{n+1})\mathbf{U}^{\mathrm{e}}_{n+1}\} \cdot \bar{\mathbf{T}}'_{n+1} + ([\mathbf{U}^{\mathrm{e}}]^{-1}_{n+1}\overset{*}{\mathbf{U}}{}^{\mathrm{e}}_{n+1}) \cdot \bar{\mathbf{T}}'_{n+1} \tag{A8}$$

Since $\mathbf{U}^{\mathrm{e}}_{n+1}$ and $\bar{\mathbf{E}}^{\mathrm{e}}_{n+1}$ commute in multiplication, $\mathbf{U}^{\mathrm{e}}_{n+1}$ and $\bar{\mathbf{T}}_{n+1}$ and hence $\mathbf{U}^{\mathrm{e}}_{n+1}$ and $\bar{\mathbf{T}}'_{n+1}$ also commute in multiplication. Thus,

$$\begin{aligned}
&\{[\mathbf{U}^{\mathrm{e}}]^{-1}_{n+1}([\mathbf{R}^{\mathrm{e}}]^{\mathrm{T}}_{n+1}\overset{*}{\mathbf{R}}{}^{\mathrm{e}}_{n+1})\mathbf{U}^{\mathrm{e}}_{n+1}\} \cdot \bar{\mathbf{T}}'_{n+1} \\
&\quad = \{[\mathbf{R}^{\mathrm{e}}]^{\mathrm{T}}_{n+1}\overset{*}{\mathbf{R}}{}^{\mathrm{e}}_{n+1}\} \cdot \{[\mathbf{U}^{\mathrm{e}}]^{-1}_{n+1}\bar{\mathbf{T}}'_{n+1}\mathbf{U}^{\mathrm{e}}_{n+1}\} \\
&\quad = \{[\mathbf{R}^{\mathrm{e}}]^{\mathrm{T}}_{n+1}\overset{*}{\mathbf{R}}{}^{\mathrm{e}}_{n+1}\} \cdot \bar{\mathbf{T}}'_{n+1} \\
&\quad = 0
\end{aligned} \tag{A9}$$

where the skew symmetry of $[\mathbf{R}^{\mathrm{e}}]^{\mathrm{T}}_{n+1}\overset{*}{\mathbf{R}}{}^{\mathrm{e}}_{n+1}$ and symmetry of $\bar{\mathbf{T}}'_{n+1}$ were taken into account. The following simplified equation is finally obtained from Equation (A8),

$$([\mathbf{F}^{\mathrm{e}}]^{-1}_{n+1}\overset{*}{\mathbf{F}}{}^{\mathrm{e}}_{n+1}) \cdot \bar{\mathbf{T}}'_{n+1} = ([\mathbf{U}^{\mathrm{e}}]^{-1}_{n+1}\overset{*}{\mathbf{U}}{}^{\mathrm{e}}_{n+1}) \cdot \bar{\mathbf{T}}'_{n+1} \tag{A10}$$

Using the diagonal representation of the symmetric tensor $\mathbf{U}^{\mathrm{e}}_{n+1}$, one can write

$$\mathbf{U}^{\mathrm{e}}_{n+1} = \mathbf{Q}_{n+1}\mathbf{\Lambda}_{n+1}\mathbf{Q}^{\mathrm{T}}_{n+1} \tag{A11}$$

where $\mathbf{\Lambda}_{n+1}$ is a diagonal tensor and $\mathbf{Q}_{n+1}$ is a rotation tensor. Therefore,

$$\overset{*}{\mathbf{U}}{}^{\mathrm{e}}_{n+1} = \mathbf{Q}_{n+1}\overset{*}{\mathbf{\Lambda}}_{n+1}\mathbf{Q}^{\mathrm{T}}_{n+1} + 2\,\mathrm{sym}(\overset{*}{\mathbf{Q}}_{n+1}\mathbf{Q}^{\mathrm{T}}_{n+1}\mathbf{U}^{\mathrm{e}}_{n+1}) \tag{A12}$$

Since $\mathbf{U}^{\mathrm{e}}_{n+1}$ and $\bar{\mathbf{T}}'_{n+1}$ commute in multiplication and both are symmetric, $(\mathbf{U}^{\mathrm{e}}_{n+1})^{-1}\bar{\mathbf{T}}'_{n+1}$ is symmetric. Since $\overset{*}{\mathbf{Q}}_{n+1}\mathbf{Q}^{\mathrm{T}}_{n+1}$ is skew symmetric and $\bar{\mathbf{T}}'_{n+1}$ symmetric, the following equation holds:

$$\{[\mathbf{U}^{\mathrm{e}}]^{-1}_{n+1}\,\mathrm{sym}(\overset{*}{\mathbf{Q}}_{n+1}\mathbf{Q}^{\mathrm{T}}_{n+1}\mathbf{U}^{\mathrm{e}}_{n+1})\} \cdot \bar{\mathbf{T}}'_{n+1} = 0 \tag{A13}$$

Thus using Equations (A12) and (A13), one can write

$$([\mathbf{U}^{\mathrm{e}}]^{-1}_{n+1}\overset{*}{\mathbf{U}}{}^{\mathrm{e}}_{n+1}) \cdot \bar{\mathbf{T}}'_{n+1} = (\mathbf{Q}_{n+1}\overset{*}{\mathbf{\Lambda}}_{n+1}\mathbf{\Lambda}^{-1}_{n+1}\mathbf{Q}^{\mathrm{T}}_{n+1}) \cdot \bar{\mathbf{T}}'_{n+1} \tag{A14}$$

Similarly, one can write the following:

$$\bar{\mathbf{E}}^{\mathrm{e}}_{n+1} = \ln(\mathbf{U}^{\mathrm{e}}_{n+1}) = \mathbf{Q}_{n+1}\ \ln(\mathbf{\Lambda}_{n+1})\mathbf{Q}^{\mathrm{T}}_{n+1} \tag{A15}$$

$$\overset{*}{\bar{\mathbf{E}}}^{\mathrm{e}}_{n+1} = \mathbf{Q}_{n+1}\overset{*}{\mathbf{\Lambda}}_{n+1}\mathbf{\Lambda}^{-1}_{n+1}\mathbf{Q}^{\mathrm{T}}_{n+1} + 2\,\mathrm{sym}(\overset{*}{\mathbf{Q}}_{n+1}\,\mathbf{Q}^{\mathrm{T}}_{n+1}\bar{\mathbf{E}}^{\mathrm{e}}_{n+1}) \tag{A16}$$

with

$$\mathrm{sym}(\overset{*}{\mathbf{Q}}_{n+1}\,\mathbf{Q}^{\mathrm{T}}_{n+1}\bar{\mathbf{E}}^{\mathrm{e}}_{n+1})\cdot\bar{\mathbf{T}}'_{n+1} = 0 \tag{A17}$$

Therefore using Equations (A16) and (A17), one derives the following:

$$\overset{*}{\bar{\mathbf{E}}}^{\mathrm{e}}{}_{n+1}\cdot\bar{\mathbf{T}}'_{n+1} = (\mathbf{Q}_{n+1}\overset{*}{\mathbf{\Lambda}}_{n+1}\mathbf{\Lambda}^{-1}_{n+1}\mathbf{Q}^{\mathrm{T}}_{n+1})\cdot\bar{\mathbf{T}}'_{n+1} \tag{A18}$$

Combining Equations (A14) and (A18), one can write the following:

$$([\mathbf{U}^{\mathrm{e}}]^{-1}_{n+1}\overset{*}{\mathbf{U}}^{\mathrm{e}}{}_{n+1})\cdot\bar{\mathbf{T}}'_{n+1} = \overset{*}{\bar{\mathbf{E}}}^{\mathrm{e}}{}_{n+1}\cdot\bar{\mathbf{T}}'_{n+1} \tag{A19}$$

Also following Equation (25) and using $\overset{*}{\bar{\mathbf{T}}}'_{n+1} = 2\mathscr{G}\,\overset{*}{\bar{\mathbf{E}}}^{\mathrm{e}\prime}_{n+1}$, one can write

$$\overset{*}{\tilde{\sigma}}_{n+1} = \frac{3\mathscr{G}}{\tilde{\sigma}_{n+1}}\,\overset{*}{\bar{\mathbf{E}}}^{\mathrm{e}\prime}_{n+1}\cdot\bar{\mathbf{T}}'_{n+1} = \frac{3\mathscr{G}}{\tilde{\sigma}_{n+1}}\,\overset{*}{\bar{\mathbf{E}}}^{\mathrm{e}}{}_{n+1}\cdot\bar{\mathbf{T}}'_{n+1} \tag{A20}$$

The following simplification is obtained using Equations (A10), (A19) and (A20):

$$([\mathbf{F}^{\mathrm{e}}]^{-1}_{n+1}\overset{*}{\mathbf{F}}^{\mathrm{e}}_{n+1})\cdot\bar{\mathbf{T}}'_{n+1} = \overset{*}{\bar{\mathbf{E}}}^{\mathrm{e}}_{n+1}\cdot\bar{\mathbf{T}}'_{n+1} = \frac{\tilde{\sigma}_{n+1}}{3\mathscr{G}}\,\overset{*}{\tilde{\sigma}}_{n+1} \tag{A21}$$

Taking the dot product of Equation (A22) with $\bar{\mathbf{T}}'_{n+1}$ and using Equations (14), (25) and (A21), results in the following:

$$\mathbf{G}_{n+1}\cdot\bar{\mathbf{T}}'_{n+1} = \overset{*}{\tilde{\sigma}}_{n+1}\left\{\frac{\tilde{\sigma}_{n+1}}{3\mathscr{G}} + \frac{2\,\tilde{\sigma}_{n+1}a_{n+1}}{3} + \frac{2\,\tilde{\sigma}^2_{n+1}b_{n+1}}{3}\right\} \tag{A22}$$

and thus $\overset{*}{\tilde{\sigma}}_{n+1}$ is finally expressed as

$$\overset{*}{\tilde{\sigma}}_{n+1} = \frac{3\mathscr{G}\mathbf{G}_{n+1}\cdot\bar{\mathbf{T}}'_{n+1}}{\tilde{\sigma}_{n+1}(1 + 2\mathscr{G}(a_{n+1} + \tilde{\sigma}_{n+1}b_{n+1}))} \tag{A23}$$

Let us now define the following tensor (function of $\overset{*}{\mathbf{F}}^{\mathrm{e}}_{n+1}$):

$$\mathbf{H}_{n+1} = [\mathbf{F}^{\mathrm{e}}]^{-1}_{n+1}\overset{*}{\mathbf{F}}^{\mathrm{e}}_{n+1} + 2\mathscr{G}a_{n+1}\overset{*}{\bar{\mathbf{E}}}^{\mathrm{e}}_{n+1} \tag{A24}$$

Using this definition and Equations (A2), (A3), (A7), Equation (41) can now be simplified as follows:

$$\mathbf{H}_{n+1} = \mathbf{G}_{n+1} + \frac{2\mathscr{G}a_{n+1}\,\mathrm{tr}(\mathbf{G}_{n+1})}{3}\mathbf{I} - \frac{3\mathscr{G}b_{n+1}\mathbf{G}_{n+1}\cdot\bar{\mathbf{T}}'_{n+1}}{\tilde{\sigma}_{n+1}(1 + 2\mathscr{G}(a_{n+1} + \tilde{\sigma}_{n+1}b_{n+1}))}\,\bar{\mathbf{T}}'_{n+1} \tag{A25}$$

Table A1. Material parameters for Al 1100-O at an initial temperature 673 K.

Material parameter	Value
A	$1.90593 \times 10^7\ \mathrm{s}^{-1}$
Q/R	$2.1086 \times 10^4\ \mathrm{K}^{-1}$
ξ	7.0
m	0.23348
s_0	29.7 MPa
h_0	1115.6 MPa
a	1.3
$\tilde{s}$	18.92 MPa
n	0.07049
$\mathscr{G}$	20.2 GPa
$\mathscr{K}$	66.0 GPa

or finally as

$$\mathbf{H}_{n+1} = \mathbf{D}_{n+1} + \frac{2\mathscr{G}a_{n+1}\,\mathrm{tr}(\mathbf{D}_{n+1})}{3}\mathbf{I} - \frac{3\mathscr{G}b_{n+1}\mathbf{D}_{n+1}\cdot\bar{\mathbf{T}}'_{n+1}}{\tilde{\sigma}_{n+1}(1+2\mathscr{G}(a_{n+1}+\tilde{\sigma}_{n+1}b_{n+1}))}\bar{\mathbf{T}}'_{n+1}$$
$$-\mathbf{C}_{n+1} + \frac{3\mathscr{G}b_{n+1}\mathbf{C}_{n+1}\cdot\bar{\mathbf{T}}'_{n+1}}{\tilde{\sigma}_{n+1}(1+2\mathscr{G}(a_{n+1}+\tilde{\sigma}_{n+1}b_{n+1}))}\bar{\mathbf{T}}'_{n+1} \tag{A26}$$

Notice that $\mathbf{D}_{n+1}$ is linearly related with $\overset{*}{\mathbf{F}}_{n+1}$ and $\mathbf{C}_{n+1}$ is independent of $\overset{*}{\mathbf{F}}_{n+1}$. With the definition of $\mathbf{H}_{n+1}$ from Equation (A24), one can transform Equation (A26) to the form of Equation (42). Also, given $\overset{*}{\mathbf{F}}_{n+1}$ and using the definition of $\mathbf{D}_{n+1}$ and $\mathbf{C}_{n+1}$ from Equations (A1) and (36), Equation (42) can be solved numerically to obtain $\overset{*}{\mathbf{F}}^{\mathrm{e}}_{n+1}$.

APPENDIX B. CONSTITUTIVE MODEL FOR Al-1100 AT 673 K

The constitutive model for 1100-Al at $\theta = 673$ K is here taken from [27]. The flow function f is given as follows:

$$f(\sigma, s, \theta) = A\exp\left(-\frac{Q}{R\theta}\right)\left[\sinh\left(\xi\frac{\sigma}{s}\right)\right]^{1/m} \tag{B1}$$

and the hardening function g is given by

$$g(\sigma, s, \theta) = h(\sigma, s)f(\sigma, s, \theta) \tag{B2}$$

where the function h is defined as follows:

$$h(\sigma, s) = h_0|1 - s/s^*|^a \tag{B3}$$

with

$$s^* = \tilde{s}\left[\frac{f(\sigma, s, \theta)}{A}\exp\left(\frac{Q}{R\theta}\right)\right]^n \tag{B4}$$

The specific values of the mechanical and thermal parameters are given in Table A1.

ACKNOWLEDGEMENTS

The work presented here was funded by NSF grant DMII-9522613 to Cornell University. Additional support was provided by the Materials and Manufacturing Directorate of the Air Force Research Laboratory at Wright-Patterson Air Force Base and by Alcoa Laboratories (Dr. Paul Wang, project manager). The computing was supported by the Cornell Theory Center. The present design simulator was developed using the object-oriented environment of *Diffpack*. The academic license that allowed us to use the various libraries of *Diffpack* is acknowledged.

REFERENCES

1. Kobayashi S, Oh S, Altan T. *Metal Forming and the Finite-Element Method*. Oxford University Press: New York, 1989.
2. Tsay J, Arora JS. Non-linear structural design sensitivity analysis for path-dependent problems, Parts I and II: General theory and analytical example problems. *Computer Methods in Applied Mechanics and Engineering* 1990; **81**: 183–228.
3. Tortorelli D. Sensitivity analysis for non-linear constrained elastostatic systems. *International Journal for Numerical Methods in Engineering* 1992; **33**:1643–1660.
4. Vidal CA, Haber RB. Design sensitivity analysis for rate-independent elastoplasticity. *Computer Methods in Applied Mechanics and Engineering* 1993; **107**:393–431.
5. Lee TH, Arora JS. Shape design sensitivity analysis of viscoplastic structures. *Computer Methods in Applied Mechanics and Engineering* 1993; **108**:237–259.
6. Kleiber M, Antúnez H, Hien TD, Kowalczyk P. *Parameter Sensitivity in Nonlinear Mechanics: Theory and Finite Element Computations*. Wiley: New York, 1997.
7. Noor AK, Needleman A, Peters JM. Sensitivity analysis for failure and damage in dynamically loaded tensile bars. *Computer Methods in Applied Mechanics and Engineering* 1998; **151**:461–478.
8. Antúnez HJ, Kleiber M. Sensitivity analysis of metal forming processes involving frictional contact in steady state. *Journal of Materials Processing Technology* 1996; **60**:485–491.
9. Antúnez HJ, Kleiber M. Sensitivity of forming processes to shape parameters. *Computer Methods in Applied Mechanics and Engineering* 1996; **137**:189–206.
10. Antúnez HJ. Thermo-mechanical modelling and sensitivity analysis for metal forming operations. *Computer Methods in Applied Mechanics and Engineering* 1998; **161**:113–125.
11. Mahnken R, Stein E. Parameter identification for finite deformation elasto-plasticity in principal directions. *Computer Methods in Applied Mechanics and Engineering* 1997; **147**:17–39.
12. Karaoglan L, Noor AK. Sensitivity analysis of frictional contact response of axisymmetric composite structures. *Computers and Structures* 1995; **55**(6):937–954.
13. Ghouali MA, Duvaut G, Ortola S, Oster A. Local analytical design sensitivity analysis of the forging problem using FEM. *Computer Methods in Applied Mechanics and Engineering* 1998; **163**:55–70.
14. Fourment L, Chenot JL. Optimal design for non-steady state metal forming processes—I. Shape optimization method. *International Journal for Numerical Methods in Engineering* 1996; **39**:33–50.
15. Fourment L, Balan T, Chenot JL. Optimal design for non-steady state metal forming processes—II. Application of shape optimization in forging. *International Journal for Numerical Methods in Engineering* 1996; **39**:51–65.
16. Zhao G, Wright E, Grandhi RV. Preform Die shape design in metal forming using an optimization method. *International Journal for Numerical Methods in Engineering* 1997; **40**:1213–1230.
17. Joun MS, Hwang SM. Die shape optimal design in three dimensional shape metal extrusion by the finite element method. *International Journal for Numerical Methods in Engineering* 1998; **41**:311–335.
18. Chung SH, Hwang SM. Optimal process design in non-isothermal non-steady metal forming by the finite element method. *International Journal for Numerical Methods in Engineering* 1998; **42**:1343–1390.
19. Coons SA. Surfaces for computer-aided design of space figures, *ESL 9442-M-139*, MIT, 1969.
20. Bézier PE. *Numerical Control—Mathematics and Applications*. Wiley: London, 1972.
21. Schumaker LL. *Spline Functions: Basic Theory*. Wiley: New York, 1981.

22. Gunasekera JS. *CAD/CAM of Dies*. Halsted Press: New York, 1989.
23. Fletcher R. *Practical Methods of Optimization*. Wiley: New York, 1987.
24. Badrinarayanan S, Zabaras N. A sensitivity analysis for the optimal design of metal forming processes. *Computer Methods in Applied Mechanics and Engineering* 1996; **129**:319–348.
25. Badrinarayanan S, Constantinescou A, Zabaras N. Preform design in metal forming. In *Numiform'95: Simulation of Materials Processing*: *Theory*, *Methods and Applications*, Shen S-F, Dawson P (eds). Balkema: Rotterdam, 1995; 533–538.
26. Weber G, Anand L. Finite deformation constitutive equations and a time integration procedure for isotropic, hyperelastic–viscoplastic solids. *Computer Methods in Applied Mechanics and Engineering* 1990; **79**:173–202.
27. Brown SB, Kim KH, Anand L. An internal variable constitutive model for hot working of metals. *International Journal of Plasticity* 1989; **5**:95–130.
28. Zabaras N, Srikanth A. An object oriented programming approach to the Lagrangian FEM analysis of large inelastic deformations and metal forming processes. *International Journal for Numerical Methods in Engineering* 1999; **45**(4):399–445.
29. Laursen TA, Simo JC. On the formulation and numerical treatment of finite deformation frictional contact problems. In: *Nonlinear Computational Mechanics—State of the Art*, Wriggers P, Wager W (eds). Springer: Berlin, 1991; 716–736.
30. Simo JC, Laursen TA. An augmented Lagrangian treatment of contact problems involving friction. *Computers and Structures* 1992; **42**(1):97–116.
31. Simo JC, Hughes, TJR. *Computational Inelasticity*. Springer: New York, 1998.
32. Zabaras N, Srikanth A. Using objects to model finite deformation plasticity. *Engineering with Computers* 1999; **15**:37–60.
33. Srikanth A, Zabaras N. Preform design and shape optimization in metal forming processes. *Computer Methods in Applied Mechanics and Engineering*, 2000, in press.
34. Srikanth A, Zabaras N. A gradient based optimization framework for the design of single and multi-stage metal forming processes. In *Symposium on Advances in Metal Forming*, Cao J, Liu WK, Xia CZ (eds). ASME, 2000, in press.

